Neurobiology of Disease 134 (2020) 104683

Contents lists available at ScienceDirect

Neurobiology of Disease

journal homepage: www.elsevier.com/locate/ynbdi

Tau overexpression exacerbates neuropathology after repeated mild head impacts in male mice

Hank Cheng, Lisa M. Deaton, Minhua Qiu, Sukwon Ha, Reynand Pacoma, Jianmin Lao, Valerie Tolley, Rita Moran, Amber Keeton, John R. Lamb, John Fathman, John R. Walker, Andrew M. Schumacher*

Department of General Medical Biology, Genomics Institute for the Novartis Research Foundation, San Diego, CA 92121, USA

ARTICLE INFO

Keywords:
Traumatic brain injury
Chronic traumatic encephalopathy
White matter
Tau
Neuroinflammation

ABSTRACT

Repeated mild traumatic brain injury (rmTBI) can lead to development of chronic traumatic encephalopathy (CTE), which is characterized by progressive neurodegeneration with presence of white matter damage, gliosis and hyper-phosphorylated tau. While animal models of rmTBI have been documented, few characterize the molecular pathogenesis and expression profiles of relevant injured brain regions. Additionally, while the usage of transgenic tau mice in rmTBI is prevalent, the effects of tau on pathological outcomes has not been well studied. Here we characterized a 42-impact closed-head rmTBI paradigm on 3–4 month old male C57BL/6 (WT) and Tau-overexpressing mice (Tau58.4). This injury paradigm resulted in chronic gliosis, T-cell infiltration, and demyelination of the optic nerve and associated white matter tracts at 1-month post-injury. At 3-months post-injury, Tau58.4 mice showed progressive neuroinflammation and neurodegeneration in multiple brain regions compared to WT mice. Corresponding to histopathology, RNAseq of the optic nerve tract at 1-month post-injury showed significant upregulation of inflammatory pathways and downregulation of myelin synthetic pathways in both genotypes. However, Tau58.4 mice showed additional changes in neurite development, protein processing, and cell stress. Comparisons with published transcriptomes of human Alzheimer's Disease and CTE revealed common signatures including neuroinflammation and downregulation of protein phosphatases. We next investigated the demyelination and T-cell infiltration phenotypes to determine whether these offer potential avenues for therapeutic intervention. Tau58.4 mice were treated with the histamine H3 receptor antagonist GSK239512 for 1-month post-injury to promote remyelination of white matter lesions. This restored myelin gene expression to sham levels but failed to repair the histopathologic lesions. Likewise, injured T-cell-deficient Rag2/Il2rg (R2G2) mice also showed evidence for inflammation and loss of myelin. However, unlike immune-competent mice, R2G2 mice had altered myeloid cell gene expression and fewer demyelinated lesions. Together this data shows that rmTBI leads to chronic white matter inflammatory demyelination and axonal loss exacerbated by human tau overexpression but suggests that immune-suppression and remyelination alone are insufficient to reverse damage.

1. Introduction

Chronic traumatic encephalopathy (CTE) is an untreatable progressive neurodegenerative disease caused by repeated head impacts (rmTBI) that gained prominent attention following its discovery in professional American football players (Omalu et al., 2005). Over the past decade, the histopathology of CTE has been extensively studied in postmortem human brains but understanding of the molecular pathogenesis of the disease is still lacking. Histopathological characteristics of CTE include tau-immunopositive neurofibrillary tangles, glial tangles, and neuropil threads commonly localized to perivascular blood vessels in the cerebral sulcal depths (Baugh et al., 2012; Stein et al., 2014; McKee et al., 2015). Gliosis, axonal damage, and white matter lesions are also present (McKee et al., 2015; Holleran et al., 2017; Alosco et al., 2017) and are characteristic of neuroinflammatory processes that can contribute to the pathogenesis of other

* Corresponding author.
E-mail addresses: hcheng@gnf.org (H. Cheng), Ldeaton@gnf.org (L.M. Deaton), Mqiu@gnf.org (M. Qiu), Sha@gnf.org (S. Ha), Rpacoma@gnf.org (R. Pacoma), Jlao@gnf.org (J. Lao), Vtolley@gnf.org (V. Tolley), Rmoran@gnf.org (R. Moran), Akeeton@gnf.org (A. Keeton), Jfathman@gnf.org (J. Fathman), Jwalker@gnf.org (J.R. Walker), aschumacher@gnf.org (A.M. Schumacher).

https://doi.org/10.1016/j.nbd.2019.104683
Received 15 July 2019; Received in revised form 22 October 2019; Accepted 20 November 2019
Available online 23 November 2019

neurodegenerative disorders such as Alzheimer's Disease (AD) (Giunta et al., 2012; Nemetz et al., 1999). It is currently unknown what role immune cells play in CTE, although human studies and rodent models of TBI have implicated microglia, macrophages, neutrophils, and T-cells (Makinde et al., 2017; Cherry et al., 2016; McKee and Lukens, 2016; Nizamutdinov and Shapiro, 2017; Bai et al., 2017).

In vivo models of rmTBI have been developed over recent years utilizing amyloid or tau-overexpressing transgenic mice, and varying the number of hits delivered, inter-impact period, anesthesia usage, and impact method (Turner et al., 2015a; Turner et al., 2015b; Galgano et al., 2015). Like how most human concussions occur, these models generally utilize a closed-headed rodent system that does not result in gross structural brain damage. Several of these models recapitulate key CTE features including gliosis, axonal injury, and white matter degeneration, often involving the visual system (Holleran et al., 2017; Petraglia et al., 2014; Ojo et al., 2016; Tagge et al., 2018; Namjoshi et al., 2014; Tzekov et al., 2014; Xu, 2015; Xu et al., 2016; Winston et al., 2016; Evanson et al., 2018; Briggs et al., 2016). White matter abnormalities are notable because they are present in all reported stages of human CTE (McKee et al., 2015), and the white matter myelin tracts can be chronically altered in humans who have suffered concussions (Johnson et al., 2013; Multani et al., 2016). These abnormalities can result in long-term neuropsychiatric symptoms of CTE and vision loss (Alhilali et al., 2015; Armstrong, 2018). Lacking, however, are in-depth regional histopathological and global gene expression analyses of brain regions most susceptible to rmTBI, including how tauopathy may influence pathology progression. This is exemplified by the relative dearth of studies that profile molecular and transcriptional signatures of CTE in human patients and animal models. Furthermore, endogenous mouse tau is less aggregation prone than human tau (Andorfer et al., 2003), which may affect tissue responses to rmTBI. Thus, comparing wild-type mice to human tau-overexpressing mice may be useful for evaluate the role of tau in neuropathogenesis following rmTBI.

While the role of tau reduction in altering rmTBI-mediated white matter outcomes has been explored (Cheng et al., 2014), studies are needed to better understand the underlying molecular role of tau in rmTBI-driven neuropathology. In the current study, we present an in-depth histopathological and transcriptomic characterization of a closed-headed rmTBI model in both C57BL/6 wild-type (WT) and Tau58.4 homozygous male mice without anesthesia. The Tau58.4 mouse line overexpresses P301S (0N4R isoform) human tau (MAPT) driven by the Thy1.2 promoter and develops progressive tauopathy from brainstem at 3 months (mo), to cortex and hippocampus by 10mo (van Eersel et al., 2015; Yin et al., 2017). Overexpression of human tau is important in the study of rmTBI because endogenous mouse tau does not normally aggregate in vivo (Andorfer et al., 2003; Gendron and Petrucelli, 2009) and is therefore less likely to recapitulate any role of human tau in disease progression. This enables us to study how a disease-associated human tau influences neuropathological development in a rodent model. In this case, mice are subject to rmTBI in a non-anesthetized setting similar to how most human concussions are experienced. To further align the model with the human disease setting, we used 3-4mo old mice at time of impact because that age in mice is comparable to young adolescent humans who may be more likely to be exposed to head injury events through contact sports.

This experimental strategy allowed us to identify injury-prone brain regions such as the optic nerve white matter tracts and differential responses to rmTBI based on genotype. Furthermore, transcriptional profiles from injured mice led us to investigate the potential utility of inflammatory and myelination pathways as nodes for intervention to modulate the progression of disease. Specifically, we attempt to use GSK239512, a myelination-inducing compound, and Rag2/il2rg knockout mice, an immunocompromised strain lacking lymphocytes, to determine if targeting these pathways would result in altered pathology. Altogether, our study methodically profiles histopathology and gene expression in rmTBI-exposed mice to show that reported myelination-promoting compounds and lymphocyte suppression alone are insufficient to repair injury.

2. Materials and methods

2.1. Animals

In this study, 3-4mo old male WT C57BL/6 (The Jackson Laboratory, Bar Harbor, US), Tau58.4 mice (Novartis Institute for Biomedical Research, Cambridge, US), and Rag2-Il2rg mice (Envigo, New Jersey, US) weighing 22–30 g were subject to the injury paradigm below. All study mice were group-housed 3–5/cage and maintained in the Genomics Institute for the Novartis Research Foundation (GNF) vivarium. Tau58.4 mice cohorts were generated by burst breeding in-house for study needs. Homozygosity of initial Tau58.4 mouse breeders was confirmed by genotyping (Transnetyx, Cordova, US) and back-crossing to C57BL/6 background strain. Mice were provided with standard mouse chow and water ad libitum and subject to 12-h light/dark cycles (light from 6 AM to 6 PM local time) in a temperature-controlled room of 22–24 °C. All procedures involving animals were conducted under Association for Assessment and Accreditation of Laboratory Animal Care (AAALAC) guidelines and approved by the Institutional Animal Care and Use Committee (IACUC) of GNF.

2.2. Injury paradigm, dosing, and schedule

For rmTBI experiments, mice were placed head first into a decapicone (BrainTree Scientific, Braintree, US) with a widened nose slit to improve head mobility and ventilation. The tail end of the decapicone was finger-sealed to prevent the mouse from moving within the bag. This ensured the animal was stable enough to forgo the need for anesthesia. The restrained animal was placed on a 5 cm thick Type E foam bed (Foam to Size Inc., Ashland, US) situated on Model 900LS stereotaxic frame (Kopf Instruments, Tujunga, US). Circular steel helmets (6 mm diameter, 3 mm thickness) were manufactured by GNF engineers and attached onto the decapicone with double-sided tape (Scotch, St. Paul, US) over the center of the mouse's head approximately 1-3 mm posterior to the eyes. Impacts were delivered by the Impact One electromagnetic impactor (Leica, Buffalo Grove, US) at 6 impacts/day for 7 days (42 total impacts), with inter-impact period of 1.5 h. 1 cohort of Tau58.4 mice was also exposed to single impact. The rationale behind selecting a 42-impact paradigm was to simulate a more frequent head injury paradigm that may be expected in competitive contact sports based on prior literature models (Petraglia et al., 2014). The impactor tip was zeroed at the contact point with the helmet. The strike velocity was 5.0 m/s, dwell time 100 ms, and impact depth 1.0 cm. Thus, the mouse head would be impacted ~1.0 cm into the foam bed, allowing for rapid acceleration-deceleration of the brain commonly observed during concussive injury. Total restraint time should not exceed 20 s. Age and genotype matched sham animals were restrained in the decapicone for 20 s without receiving an impact.

Following impacts, the mice were removed from the restraint bag, returned to their cages, and observed for 10 s to assess any behavioral or pain abnormalities. Pain scores between 1 and 4 (1 = no overt response to injury, 2 = mild response with rapid tail rising and falling prior to return to normal behavior, 3 = moderate response with sustained tail rise and dragging of forepaws, and 4 = minor convulsions or seizure) were recorded after every impact. The average pain score over the 42-impact course across studies was 1.24 ± 0.18, with most impacts resulting in no overt injury response. There were no remarkable differences in pain scores across cohorts. Because mice showed temporary forelimb weakness immediately post-injury that recovered within minutes, all rmTBI mice cages had chow and hydrogel (ClearH2O, Portland, US) placed on the floor of the cage for easy access. Cohort sizes were 5–10 per group or as noted. rmTBI-exposed mice

generally had larger sample sizes to accommodate the possibility of dropouts (seizure-induced mortality). The dropout rate across all studies was < 2%. Mice were weighed 1 day after the week-long rmTBI course (up to 10% body weight loss is normal) and again prior to euthanasia. WT, Tau58.4, and Rag2-Il2rg mice were euthanized at 1mo from last impact, or otherwise noted in the study.

For remyelination dosing studies, GSK239512 (Synnovator Inc., Durham, US) was dosed starting 3 days post-impact orally twice a day (b.i.d) at 10 mg/kg for 1mo. GSK239512 was formulated in 0.5% methyl cellulose, 0.1% Tween 80 (MC Tween) solution and dosed at a volume of 100ul. Vehicle treated rmTBI animals were dosed with MC Tween b.i.d. as a control.

2.3. Oligodendrocyte progenitor cell culture

1 day prior to cell seeding, CellCarrier-384 Ultra microplates (PerkinElmer, Waltham, US) were coated with 100 μg/ml poly-L-lysine (Sigma-Aldrich, St. Louis, US) overnight at room temperature (RT). Primary rat oligodendrocyte progenitor cells (OPC) obtained from Gibco (Cat #A30662, lot #20010535, ThermoFisher, Waltham, US) were seeded at a density of 2000 cells/well in proliferation media after plates were washed three times with phosphate buffered saline (PBS) (ThermoFisher). Proliferation media comprised of Neurobasal media, 1× B27 without vitamin A, 1× non-essential amino acid, 1× pen strep glutamine, 2-mercaptoethanol (1:1000), and 30 ng/ml PDGF-AA (Peprotech, Rocky Hill, US). All supplements except PDGF-AA were obtained from ThermoFisher. After 1 day in vitro (DIV), media was changed and 10 μM GSK239512 in 0.1% DMSO, 0.14 μM triiodothyronine (T3, Sigma-Aldrich), or vehicle (0.1% DMSO, Sigma-Aldrich) were added to fresh differentiation media (proliferation media without PDGF-AA). Compounds were dispensed into media using Echo Liquid Handler (Labcyte, San Jose, US). OPCs were treated for 5DIV, then fixed for staining and analysis.

2.4. Immunohistochemistry and histology analysis

To prepare tissues for histological applications, mice were anesthetized with 2.5% isoflurane and transcardially perfused with 15 ml of physiological saline via a syringe with 25G5/8 needle (Becton Dickinson, Franklin Lakes, US). Brains were collected and bisected at midline where the left hemisphere was fixed in 10% neutral buffered formalin (NBF) (Sigma-Aldrich) for 3 days, while the right hemisphere was microdissected into cortex and optic tract (OT) plus right optic nerve (ON) and promptly frozen on dried ice for RNA applications. The left ON was fixed in 10% NBF for 1 day. After tissues were fixed, they were transferred to 70% ethanol in preparation for paraffin embedding.

Fixed tissues were placed in cassettes for processing via the Tissue Tek VIP6 vacuumed infiltration processor (Sakura Finetek USA, Torrance, US) which dehydrates them through a series of graded ethanols and xylenes prior to infiltration with paraffin wax (Avantik, Springfield, US) at 56–58 °C. These tissues were subsequently embedded into wax blocks for sectioning. Wax blocks were loaded onto a RM2255 microtome (Leica) and cut into 5 μm thick sagittal sections. 10–20 serial sections were obtained from each ON, while 20 sections from lateral 0.5 mm, 1 mm, 1.5 mm and 2 mm were obtained from each brain.

Immunohistochemistry (IHC) was automated using the Ventana Discovery Ultra (Ventana Medical Systems, Oro Valley, US). All IHC reagents except for common lab reagents such as alcohol, and primary antibodies were obtained from Ventana. Primary antibodies and dilutions used in the study are as follow: rat GFAP (1:200; Invitrogen, Carlsbad, US), rabbit Iba1 (1:1600; Wako, Richmond, US), mouse AT8 phospho-tau (1:100; ThermoFisher), mouse BIII-Tubulin (1:100; Sigma-Aldrich), rabbit CD3 (1:150; ThermoFisher), rabbit Olig2 (1:1000; Millipore, Burlington, US), rabbit Tmem119 (1:100; Abcam, Cambridge, UK), rabbit Ki-67 (1:100; ThermoFisher), rabbit cleaved Caspase-3 (1:100; Cell Signaling, Danvers, US), mouse IgG (1:250; Jackson ImmunoResearch, West Grove, US), mouse Mbp (1:1000; ThermoFisher), rabbit T22 oligomeric Tau (1:500; Millipore). Each antibody was separately optimized by Ventana with positive control tissues of mouse spleen or Tau58.4 mouse brains. Negative controls without primary antibodies confirmed specificity. Ventana staining protocol is extensive and different for each antibody. Briefly, slides were de-paraffinized with EZ-prep and rehydrated in machine. Slides were washed with Ventana Reaction Buffer and quenched with hydrogen peroxide for 12 min. Antigen retrieval was performed with Ventana Protease 1 Enzyme or HIER-Automated Ventana CC1 depending on antibody at 37–95 °C for 30-60 min, followed by blocking with normal goat serum (1:20). Primary antibodies were applied at 37–42 °C for 1–6 h according to optimized protocol. Secondary antibodies were Ventama Omnimap for rat and rabbit primary antibodies, and Ventana MOMAP Complex for mouse primary antibodies, and were applied according to optimized dilution (1:20) at RT for 45 min. Ventana Chromomap DAB or DABMAP were used as the detection agent according to optimized primary antibody protocol. Slides were counterstained with hematoxylin (Sigma-Aldrich), coverslipped, and scanned by Nanozoomer S360 (Hamamatsu, San Diego, US) into ndpi files.

For luxol fast blue (LFB) staining, slides were deparaffinized, rehydrated, and stained in LFB solution (Acros Organics, New Jersey, US) in a 56 °C oven overnight. Slides were rinsed with 95% ethanol and water, then differentiated in lithium carbonate and 70% ethanol. After differentiation, slides were counterstained with cresyl violet (Sigma-Aldrich) for 30 s, rinsed with water, then alcohol and xylene (Sigma-Aldrich) cleaned. Coverslipped slides were scanned into ndpi Nanozoomer files.

Scanned histology images were hand annotated in Nanozoomer. Cortex, hippocampus, corpus callosum (CC), superior colliculus (SC), brainstem, OT, ON, and ON lesions were annotated in different colors depending on the stain. To prevent selection bias, entire tissue regions were annotated for analysis.

Automated cell and signal detection was performed using MATLAB 2018 software: each raw IHC stain was converted to CMYK color domain to separate stains which were then thresholded for cell and signal detection. For signal detection, threshold was computed on the stain color of interest using standard Otsu's method. For cell counting, a watershed-based approach was applied to segment the candidates. Within the brain region (cortex, hippocampus, CC, SC, brainstem, OT, ON, or ON lesions), each signal of interest was quantitated by signal/tissue area ratio, cell density was calculated as number of segmented cells normalized by tissue area. Activated microglia ratio was calculated by dividing area of microglial cell bodies by area of microglial processes.

2.5. Fluorescent staining and analysis

Immunocytochemistry on primary rat OPCs was performed by an automated HD washer (GNF Systems) using standard protocols as follow. Cells were fixed with 4% paraformaldehyde (PFA) (Alfa Aesar, Ward Hill, US) at RT for 30 min. After fixation, the cells were washed 3 times with PBS and then permeabilized with 0.15% Triton-X100 (Sigma-Aldrich), 1.5% bovine serum albumin (BSA) (Sigma-Aldrich) in PBS for 45 min. Rabbit anti-Mbp (1:1000; Abcam) was diluted in 0.15% Triton-X100, 1.5% BSA in PBS and applied onto cells overnight at RT. Next day, cells were washed 3 times with PBS and stained with Alexa Fluor 546 donkey anti-rabbit secondaries (1:1000; Life technologies) plus 0.1 μg/ml Hoechst (Sigma-Aldrich) for 3 h at RT. Lastly, cells were washed 3 times with PBS before leaving 27ul residual volume prior to image acquisition. Images were acquired using automation via the ImageXpress Confocal system (Molecular Devices, San Jose, US) at 20× magnification.

Fluoro-Jade C (FJC) (Millipore) was reconstituted in water and

freshly diluted in 0.1% acetic acid to a working concentration of 0.0001% + 1 μg/ml 4′,6-diamidino-2-phenylindole (DAPI) (ThermoFisher). All steps were performed at RT. Xylene de-paraffinized brain and ON slides were rinsed with PBS and loaded onto Sequenza racks (ThermoFisher) for staining. Slides were incubated with 0.06% potassium permanganate (Sigma-Aldrich) for 10 min and washed with water before application of FJC working solution for 10 min. After staining, slides were rinsed with distilled water for 1 min 3 times, then dried in a 50 °C slide warmer before xylene cleansing and coverslipping with Immu-mount (ThermoFisher). Image acquisition was performed with the EVOS FL Auto Imaging System (ThermoFisher) at 20× magnification.

FJC fluorescent TIFF images were analyzed blinded with ImageJ (National Institutes of Health, US). Regions of interest (CC, SC, and ONT) were annotated, then background subtraction was applied with rolling ball radius of 50pixels. Images were converted to 8-bit images and then thresholded using the ImageJ triangle method to allow quantification of the stained area without detection of the background staining. The staining was quantified as the number of FJC counts (particle size: 10–100) per mm^2 of tissue due to the punctate-like staining.

2.6. RNA processing

For RNA extraction, frozen optic nerve with optic tract (ONT) and cortex were lysed in 500 μl Trizol (ThermoFisher) and subject to homogenization using tissuelyser beads (Qiagen, Hilden, Germany) for 3 min at 30 hertz. 200 μl phenol-chloroform (ThermoFisher) was added to homogenized tissue prior to centrifugation at 21000 *g* for 10 min at RT for phase separation. 350 μl of the supernatant was transferred to a new 1.5 ml tube with 350 μl of 70% ethanol and loaded onto RNeasy spin columns from the RNeasy kits (Qiagen). The remaining protocol was executed as according to manufacturer instructions including with on-column DNase digestion. The eluted RNA was quantified using the Nanodrop 1000 (ThermoFisher) and cross-validated using a Qubit fluorimeter (ThermoFisher) to normalize sample loading quantities.

For RNAseq preparation, 200 ng of total RNA was used to produce RNAseq libraries with the Illumina TruSeq Stranded mRNA kit (Illumina, San Diego, US). Quality of the RNA and libraries were confirmed on an Agilent Tape Station (Agilent, Santa Clara, US). Libraries were run on a HiSeq 2500 (Illumina) with 50 bp single-end reads. FASTQ files were generated with the Illumina pipeline. Reads were aligned to the mouse genome using STAR. All samples contained at least 20 million mapped reads.

2.7. Quantitative polymerase chain reaction

qPCR was run using SuperScript III One-Step RT-PCR System with Platinum Taq High Fidelity DNA Polymerase (ThermoFisher) kit according to manufacturer guidelines. 20 μl reaction volumes were loaded into MicroAmp Optical 384-well reaction plates (Applied Biosystems, Foster City, US). Due to the low quantity of RNA recovered from ONT samples, only 20 ng of RNA was loaded for ONT, while 200 ng of RNA was loaded for cortex. Thermocycling program was run on a QuantStudio7 (ThermoFisher) with a hold stage of 15 min 50 °C to 2 min at 95 °C followed by 40 cycles of 15 s at 95 °C, then 60 °C for 30 s, maintaining 1.6 °C/s temperature change for each step.

All non-reference primers were Taqman assays with VIC probes. Genes and assay ID are as follow: Cd8a (Mm01182107_g1), Csf1 (Mm00432686_m1), Csfr1 (Mm01266652_m1), Cst7 (Mm00438351_m1), Gfap (Mm01253033_m1), Gpr17 (Mm02619401_s1), Gpr37 (Mm00494729_m1), Id2 (Mm00711781_m1), Il1α (Mm00439620_m1), Itgax (Mm00498701_m1), Mbp (Mm01266402_m1), Mog (Mm01279062_m1), Olig2 (Mm01210556_m1), TNFα (Mm00443258_m1). 36B4 with FAM probe was used as the reference gene. 36B4 primer (IDT, San Jose, US) sequences are as follow: Forward – 5'AGA TGC AGA TCC GCA T3', Reverse – 5'GTT CTT GCC CAT CAG CAC C3', Probe – 5'FAM/CGC TCC GAG/ ZEN/ GGA AGG CCG/ ABKFQ3'. Data calibration and quantification was done using the $2^{-\Delta\Delta CT}$ method.

2.8. Mass cytometry preparation

For mass cytometry (CyTOF), 50 μl of whole blood was collected in EDTA coated tubes (Becton Dickinson), on ice via retro-orbital bleeds prior to sacrifice. Blood was transferred to a 96-deep well V-bottom plates (Corning, Salt Lake City, US), then fixed with 1.6% PFA for 15 min at RT. Plates were then spun 500 *g* for 5 min at RT and PFA was aspirated. Blood samples were then washed twice with 1 ml 10% fetal bovine serum (FBS) (Corning) in PBS, spun down, and reconstituted in residual volume before being frozen in −80 °C for storage. All buffers, detailed protocols, and antibodies for CyTOF were acquired from Fluidigm (South San Francisco, US). Each step was followed by a 5 min spin at 500 g at 4 °C unless otherwise noted. Thawed fixed frozen blood was resuspended in 1 ml Barcode Perm buffer diluted in PBS and washed 3 times. For sample barcoding, Cell-ID 20-Plex Pd Barcoding Kit was thawed and resuspended in 100 μl barcode perm buffer prior to mixing with 900 μl of cell samples in barcode perm buffer for 45 min at RT. Samples were then washed 3 times with Fluidigm Cell Staining Buffer (staining buffer) to remove residual barcodes. All samples were then transferred from the plates and pooled into a 15 ml falcon tube and counted by Vi-CELL Automated counter (Beckman Coulter, Brea, US).

Extracellular antibodies (all except 158Gd-Foxp3) were added at a quantity of 1 μl antibody/3million cells to a final staining volume of 500 μl. Antibodies with conjugated metals are as follow: 141Pr-Ly6G, 142Nd-CD11c, 143Nd-GITR, 144Nd-CSF1R, 145Nd-CD69, 146Nd-CD8a, 147Sm-CD45.2, 148Nd-CD11b, 149Sm-CD19, 150Nd-CD25, 151Eu-CD28, 152Sm-CD3, 153Eu-PDL1, 156Gd-CD14, 158Gd-Foxp3, 159 Tb-F4/80, 162Dy-Ly6C, 164Dy-CD62L, 167Er-Nkp46, 171Yb-CD44, 172Yb-CD4, 174Yb-MHCII, 175Lu-CD127. Cells were stained for 30 min at RT on a shaker, then washed 2 times with staining buffer. Cells were then resuspended in residual volume and placed on ice for 10 min to chill, before −80 °C overnight permeabilization with 1 ml of −20 °C chilled methanol (Sigma-Aldrich). Next day, samples were rehydrated with 10 ml staining buffer. Subsequent centrifugation steps were performed at 800 *g* for 5 min. This was repeated 2 times prior to staining with intracellular antibodies 158Gd-Foxp3 plus 2 μl Cell-ID Intercalator-Ir in 500ul staining buffer for 1 h at RT. Afterwards, cells were washed twice with 10 ml of staining buffer, counted, and washed one more time with water. Pelleted samples were taken to the Helios CyTOF System for analysis.

Samples were diluted in calibration beads at a concentration of 1million cells/ml, filtered through a 40um strainer, and ran at a 30 μl/min sample induction rate, with ~300 events/s. Approximately 2million cells were analyzed in the pooled sample. Data was analyzed in Flowjo software V10 (Tree Star, Ashland, US) and further analysis including visne plots was generated in Cytobank (Cytobank, Santa Clara, US).

2.9. Statistical analysis

The sample size for each experiment specified in their respective captions. Data are expressed as mean ± SEM. Statistical analysis was performed using Student's *t*-test and one-way ANOVA with Tukey's multiple comparison post hoc test. Analyses were performed using GraphPad Prism 7 (GraphPad Software Inc) unless otherwise noted. Statistical significance was defined as $P < 0.05$, or as noted. For RNAseq analysis, adjusted *p*-values with Benjamini-Hochberg correction were calculated using the R package DESeq2. Gene ontology (GO) enrichment graphs with adjusted p-values were generated by Metascape (Zhou 2019) or by clusterProfiler (Yu et al., 2012).

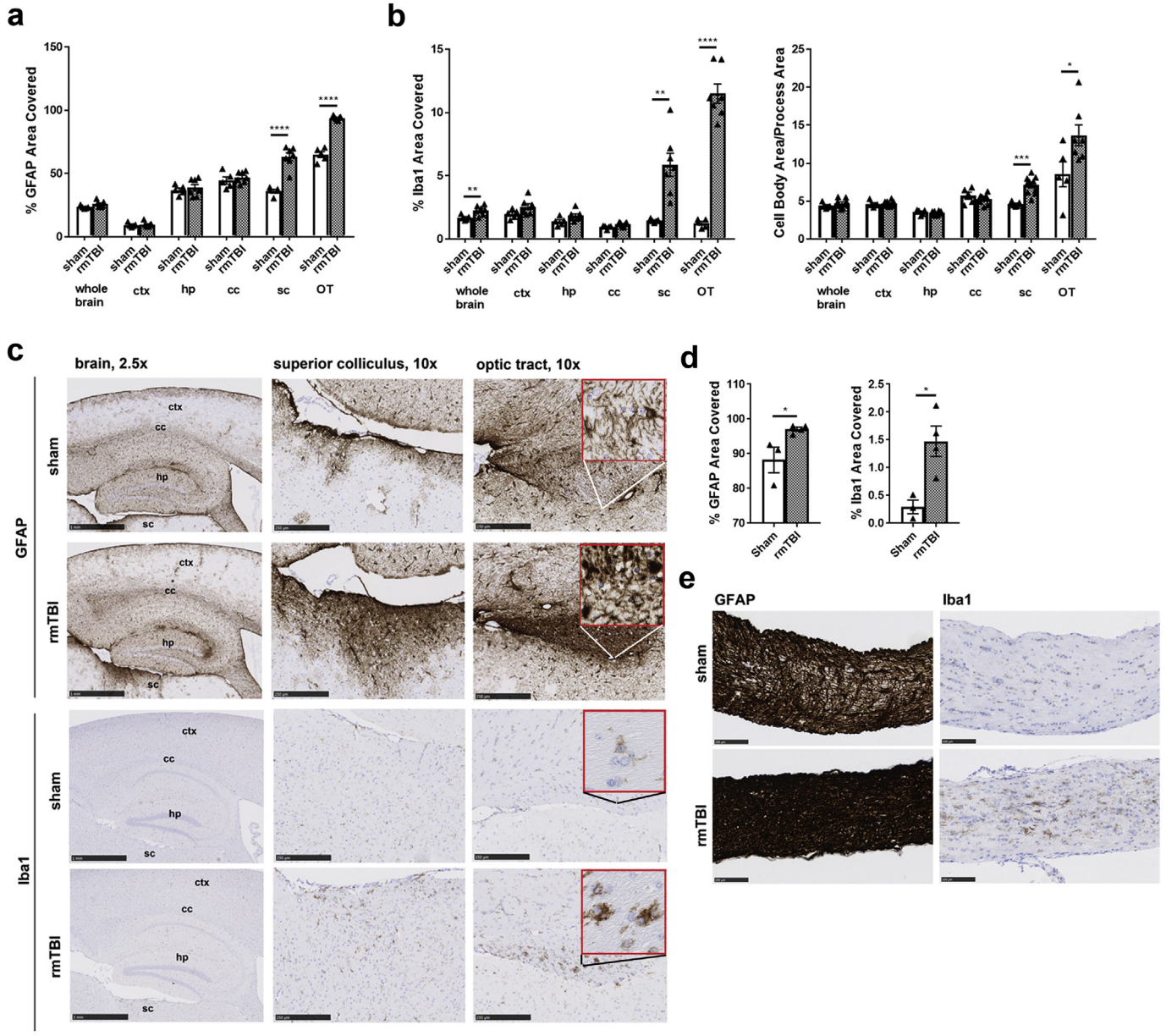

Fig. 1. Gliosis of the optic nerve tract at 1mo post-impact in injured C57BL/6 mice.
a) Quantification of GFAP coverage in ctx, hp., cc, sc, and OT in WT mice 1mo post-impact. $n = 5$ sham, $n = 7$ rmTBI. b) Quantification of Iba1 coverage and microglial activation in the same regions as a function of cell body area/process ratio. c) Representative images of ctx, hp., sc, and OT regions in WT mice stained for GFAP and Iba1. Note the enlarged activated microglial cell bodies in white matter of injured mice. Red insets denote 40× magnification to show morphology. Scale bars, 2.5×: 1 mm; 10×: 250 μm. d) Quantification of GFAP and Iba1 in the ON. $n = 3$ sham, $n = 4$ rmTBI. e) Representative images of optic nerve in WT mice stained for GFAP and Iba1. Scale bars, 100 μm.
Bar graph and error bars indicate mean ± SEM. *p < 0.05; **p < 0.01; ***p < 0.001; ****p < 0.0001 vs sham by two-tailed Student's t-test. Ctx = cortex, hp. = hippocampus, cc = corpus callosum, sc = superior colliculus, OT = optic tract, ON = optic nerve.

3. Results

3.1. rmTBI induces neuroinflammation and demyelination of the optic nerve tract in wild type mice

We first wanted to characterize the neuropathology and susceptibility of different brain regions in a mouse model of rmTBI. To do this, the effects of rmTBI on the whole WT brain were analyzed 1- and 3mo after repeated impact injury. At 1mo post-injury, astrocytic GFAP and microglial Iba1 were selectively increased in the optic tract (OT) and superior colliculus (SC), indicating gliosis in the visual system's white matter tracts of the brain (Fig. 1a-c). Morphological analysis of microglia based on cell body area to process area ratio showed a significant increase in reactive microglia in the OT, but not cortex or hippocampus (Fig. 1b). This white matter inflammation drives a modest increase of Iba1 in the whole brain.

Since the visual system was implicated in the brain, the responses of the optic nerve (ON) to rmTBI were investigated. Like in the brain, GFAP and Iba1 were significantly increased in the injured ON (Fig. 1d,e). These observations corresponded to a gene expression increase of Gfap in optic nerve + optic tract (ONT), but not in the cortex. The cytokines Tnfα and Il1α were also investigated, but showed no change in either tissue (Suppl. Fig. 1a). The gliosis was coupled to a significant increase in ONT cellularity and disorganized nuclei that contrasted with the structured linear alignment of nuclei in sham nerves (Fig. 2a). To determine if this morphology was due to active division or

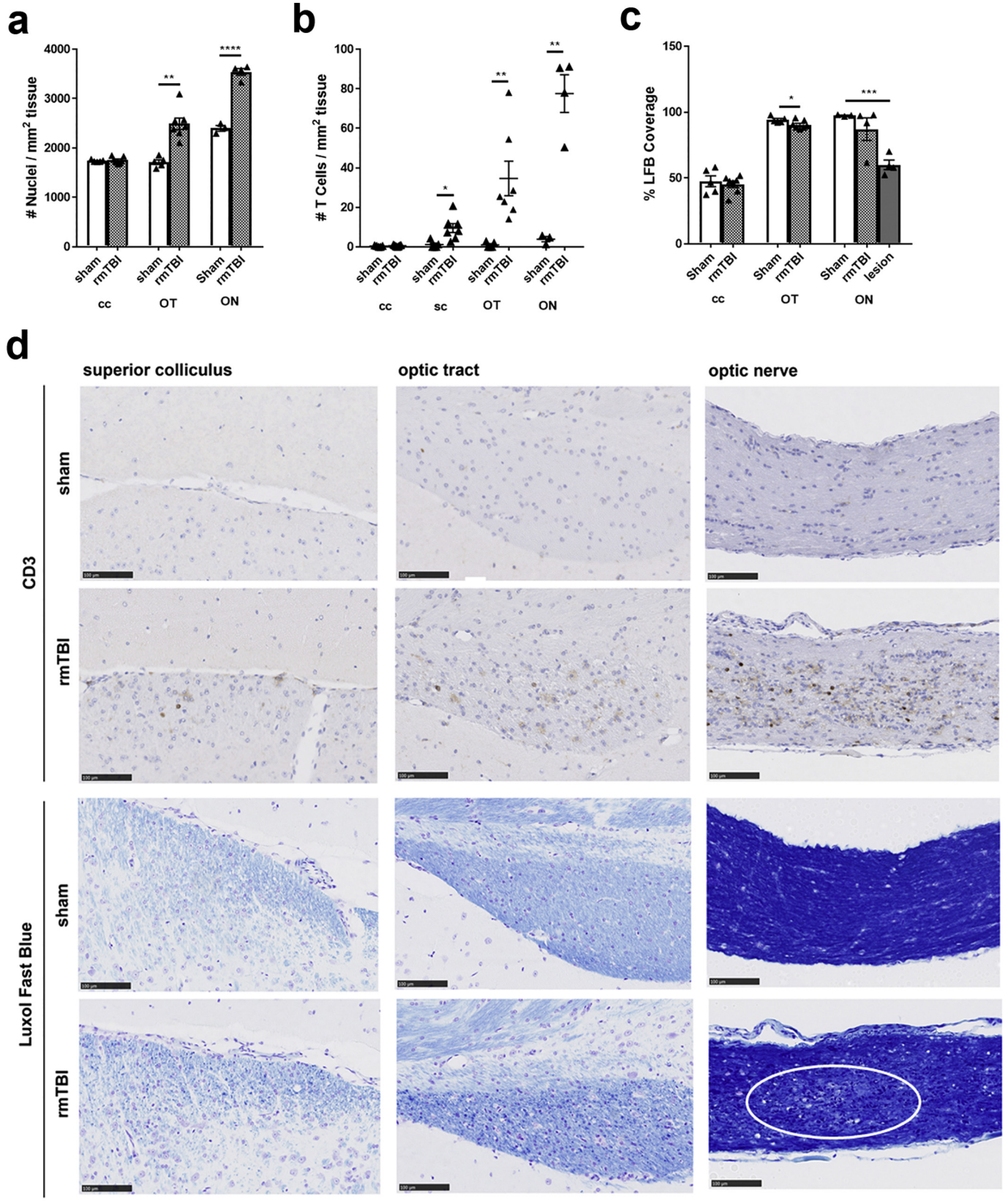

Fig. 2. T-cell infiltration and demyelination in optic nerve and tract of injured C57BL/6 mice.
a) Quantification of white matter cellularity in cc, OT, and ON as nuclei counts/mm^2 tissue. b) Quantification of CD3 expressing T-cell counts in cc, sc, OT, and ON. c) Quantification of myelin (Luxol fast blue, LFB) staining in cc, OT, and ON. LFB coverage in demyelinated lesions of the ON were also quantified for comparison. d) Representative images of sc, OT, and ON stained with CD3 and LFB. Note increased cellularity in rmTBI exposed tissue. White oval in rmTBI ON indicates a demyelinated lesion, selected based on regions of decreased LFB staining with evident T-cell co-localization. Scale bars, 100 μm.
Bar graph and error bars indicate mean ± SEM. *$p < 0.05$; **$p < 0.01$; ***$p < 0.001$ vs sham by two-tailed Student's *t*-test. (For interpretation of the references to color in this figure legend, the reader is referred to the web version of this article.)

infiltration of peripheral leukocytes, we stained for Ki67, IgG, and CD3. IgG staining was almost negligible, indicating that the blood brain barrier was not chronically compromised in injured WT mice (Suppl. Fig. 1b). There was however, an increased number of Ki67+ cells in the OT, which indicated active cell division (Suppl. Fig. 1c). CD3+ T-cells were also detected in the ONT and SC with rmTBI at 1mo (Fig. 2b), suggesting subchronic neuroinflammation of the visual system's white matter tracts with both innate and infiltrating peripheral components. As a comparator, the corpus callosum (CC) was a white matter region that did not show evidence of injury in WT mice (Fig. 2).

The presence of T-cells in white matter was reminiscent of demyelinating diseases such as multiple sclerosis (MS), so we analyzed myelin in the brain and ON by Luxol fast blue (LFB) staining. At 1mo post-injury, the ON developed focal cavernous demyelinated lesions that corresponded with an increase in infiltrating CD3+ T-cells (Fig. 2c,d). There was also detectable loss of myelin in the OT within the brain, characterized by porous LFB staining and fragmented myelin debris (Fig. 2d). These observations persisted as long as 3mo post-injury in WT mice with no evidence of neuroinflammatory progression (Suppl. Fig. 2). Since CTE is characterized as an rmTBI driven tauopathy (Omalu et al., 2005), we stained the brain and ON for phosphor-tau (AT8). However, we did not detect AT8 in any WT animals at any time point (Suppl. Fig. 3), which is unsurprising as mouse tau is known not to aggregate in vivo even after rmTBI (Gendron and Petrucelli, 2009; Laurer et al., 2001; Acabchuk et al., 2016). Taken together, rmTBI induces chronic neuroinflammation of the ONT concomitant with demyelination, but does not induce tauopathy in WT mice.

3.2. Human Tau overexpression in mice exacerbates rmTBI mediated white matter injury

Tauopathy is a key feature of clinical CTE but was not recapitulated by rmTBI in WT mice. Therefore, we subjected 3-4mo old homozygous Tau58.4 male mice to the same injury paradigm to determine if tau contributes to CTE pathology in our model. Similar to WT mice, GFAP, Iba1, and reactive microglial morphology were significantly increased in the OT and SC at 1mo post-injury (Fig. 3). However, there was further induction of cortical and CC gliosis not present in WT mice (Fig. 1 vs Fig. 3). This was consistent with increased gene expression of Gfap, Il1α, and Tnfα in the ONT, and Gfap in the cortex (Suppl. Fig. 4a). Notably, there appeared to be increased numbers of CD3 and Iba1-positive cells in the CC around the lateral ventricles, near the choroid plexus, suggesting infiltration of peripheral leukocytes into the white matter (Fig. 3d). To clarify this, we stained the ON for Tmem119, a homeostatic microglia-specific marker (Bennett et al., 2016; Zrzavy et al., 2017), and found a decrease of Tmem119 upon rmTBI (Fig. 3e). The reduced Tmem119 and Iba1 ratio in injured ON suggests a loss of homeostatic microglia and that the Iba1-expressing cells in white matter are likely peripheral myeloid cells such as macrophages.

The myeloid cell increase was accompanied by a significant increase in white matter cellularity, a 20% decrease in CC sagittal area, and CD3+ T-cell infiltration of the CC and ONT (Fig. 4). However, similar to WT, Ki67+ cells were noticeably increased only in the ONT, and not in the SC or CC (Suppl. Fig. 4b). There were also regions containing demyelinated lesions in the ON that co-localized with CD3+ T-cell densities, and an overall modest demyelination of the OT, but not CC, by LFB and MBP staining (Fig. 4b-e). In addition, there was evidence of blood brain barrier impairment, as 2/5 injured ONs showed IgG staining near lesions (Suppl. Fig. 4c). Fluoro-Jade C (FJC), a marker of degenerating neurons, was also present as puncta in the ONT and SC, but not CC (Suppl. Fig. 4d). Complementing this, we detected cleaved caspase-3 staining near lesions, indicating some apoptosis near the lesions (Suppl. Fig. 4e). Although phosphor-tau was detected in brain of Tau58.4 mice, rmTBI did not show evidence of accelerating phosphor-tau deposition in any region of the brain (Suppl. Fig. 4f). We also investigated oligomeric tau (T22 antibody) in the ON, but did not detect any expression (not shown). Finally, to ensure that repeated impacts are required for these chronic neuroinflammatory effects, five Tau58.4 mice were subject to a single impact and assessed after 1mo. There were no histopathological differences in gliosis, demyelination, or T-cell infiltration for any brain region between single-impacted mice and shams (not shown).

Unlike with WT mice, where 1- and 3mo pathology was similar, neuroinflammation was exacerbated at 3mo in Tau58.4 mice, with GFAP and Iba1 coverage increasing in grey matter-rich regions such as the hippocampus (Suppl. Fig. 5a,b). Notably different compared to the 1mo time point was the presence of FJC puncta in the CC, as well as evidence of cortical thinning, which suggest an ongoing chronic neurodegeneration in rmTBI exposed Tau58.4 mice (Suppl. Fig. 5c,d). Demyelination was also prominent, with several mice showing loss of MBP beyond focal lesions and across the entire ON (Suppl. Fig. 5e). Like the 1mo time point, however, there was no evidence of accelerated phosphor-tau deposition in Tau58.4 mice at 3mo post-injury (Suppl. Fig. 5f). This suggests that tauopathy in our model was not affected by impact-injury, and that the reported inflammation was driven by rmTBI as opposed to phosphor-tau aggregates. Notably, IgG staining was undetected in the ON lesions compared to the 1mo time point (not shown), which suggests possible BBB repair over time. Literature reports have documented transient BBB disruption occurring in the ON within 4-h of mTBI that returns to baseline within 24-h (Xu 2016), so we investigated a small subset of injured Tau58.4 mice ($n = 4$) at 1-day post-injury to assess transient effects. This time point is effectively 1 week after the first impact and interestingly, demyelinated lesions were already present with CD3 densities (Suppl. Fig. 6a). However, all mice showed IgG and cleaved caspase-3 staining near ON lesions, suggesting an acute and focal breakdown of the BBB with apoptosis that is not present in the brain white matter (Suppl. Fig. 6a,b).

3.3. rmTBI results in robust neuroinflammatory gene signatures in the ONT

To take a broader view of the molecular mechanisms that are altered with rmTBI and sensitized by tauopathy, we performed RNAseq on the cortex and ONT of both WT and Tau58.4 mice at 1mo post-rmTBI. Expression of ten times more genes were significantly altered in the Tau compared to WT ONT, respectively (3612 vs 305), with 250 overlaps (Fig. 5a). This is consistent with Tau-overexpression sensitizing the mice to injury. Conversely, only 37 genes were significantly changed in WT cortex and none in Tau58.4 cortex. Because of this, we focused on the gene signature alterations in the ONT. Hierarchal clustering of ONT samples showed that injured Tau58.4 mice were highly similar and that TBI samples tended to cluster together (Fig. 5b). The Tau transgene had a less obvious effect on sham clustering.

The most significantly changed ONT genes by rmTBI in both Tau and WT were associated with neuroinflammation and neurodegeneration, including Itgax, Apoe, Trem2, Tyrobp, and C1q. The number of downregulated genes was modest in comparison (Fig. 5c). Pathway analysis of the upregulated genes showed strong enrichment of immune activation pathways, including cytokine production, inflammatory response, T cell activation, and myeloid leukocyte activation. This corroborates the histological findings (Fig. 5d). T-cell genes such as CD3e, CD5 and CD8, but not CD4, were increased in both injured Tau and WT mice, which suggests the infiltrating CD3 T-cells in the injured ONT are likely enriched for CD8 killer T-cells (Fig. 5f).

Downregulated pathways showed strong enrichment for cholesterol biosynthesis and cellular component assembly involved in morphogenesis, and modest enrichment for dendrite development, ion transport, glutamatergic receptor pathways, and muscle system processes (Fig. 5e). This corroborates our observations of demyelination as cholesterol biosynthesis is a crucial process in which astrocytes support neurons for membrane synthesis and oligodendrocytes for myelinogenesis (Saher and Strumpf, 2015).

We were also interested in the rmTBI pathways that were

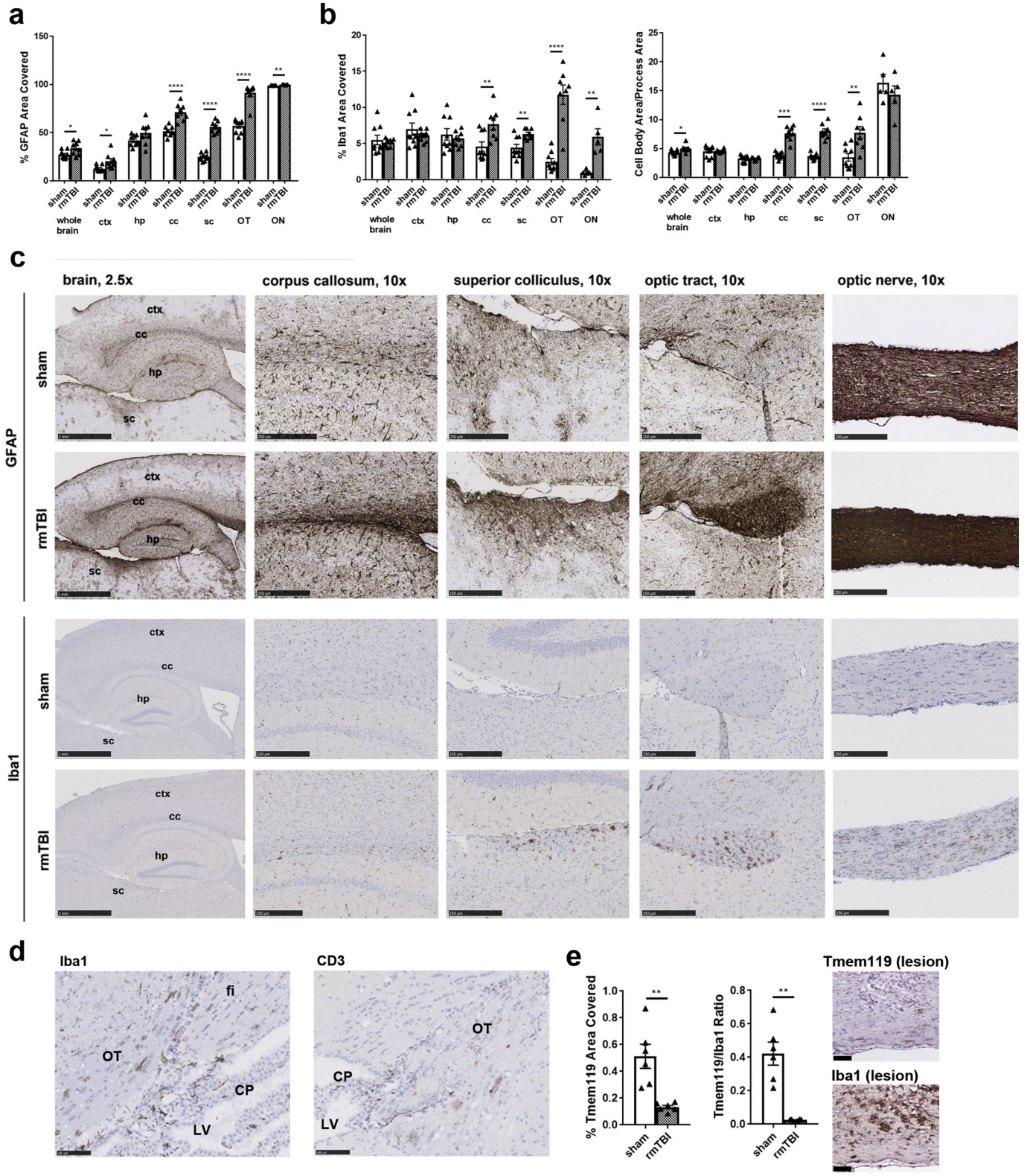

Fig. 3. Gliosis of the optic nerve tract at 1mo post-impact in injured Tau58.4 mice.

a) Quantification of GFAP coverage in ctx, hp., cc, sc, OT, and ON in Tau58.4 mice 1mo post-impact. $n = 9$ sham, $n = 8$ rmTBI, $n = 5$ optic nerves. b) Quantification of Iba1 coverage and microglial activation as a function of cell body area/process ratio in same regions. c) Representative images of ctx, hp., cc, sc, and OT regions in Tau58.4 mice stained for GFAP and Iba1. Scale bars, 2.5×: 1 mm; 10×: 250 μm. d) Images of Iba1 and CD3 expressing cells congregating in CP and OT junctions Scale bars, 100 μm. e) Image of Iba1 and Tmem119 staining in the same ON lesion with corresponding quantification of Tmem119 area coverage and Tmem119/Iba1 ratio. Scale bars, 50 μm.

Bar graph and error bars indicate mean ± SEM. *$p < 0.05$; **$p < 0.01$; ***$p < 0.001$; ****$p < 0.0001$ vs sham by two-tailed Student's *t*-test. CP = choroid plexus, fi = fimbria, LV = lateral ventricle.

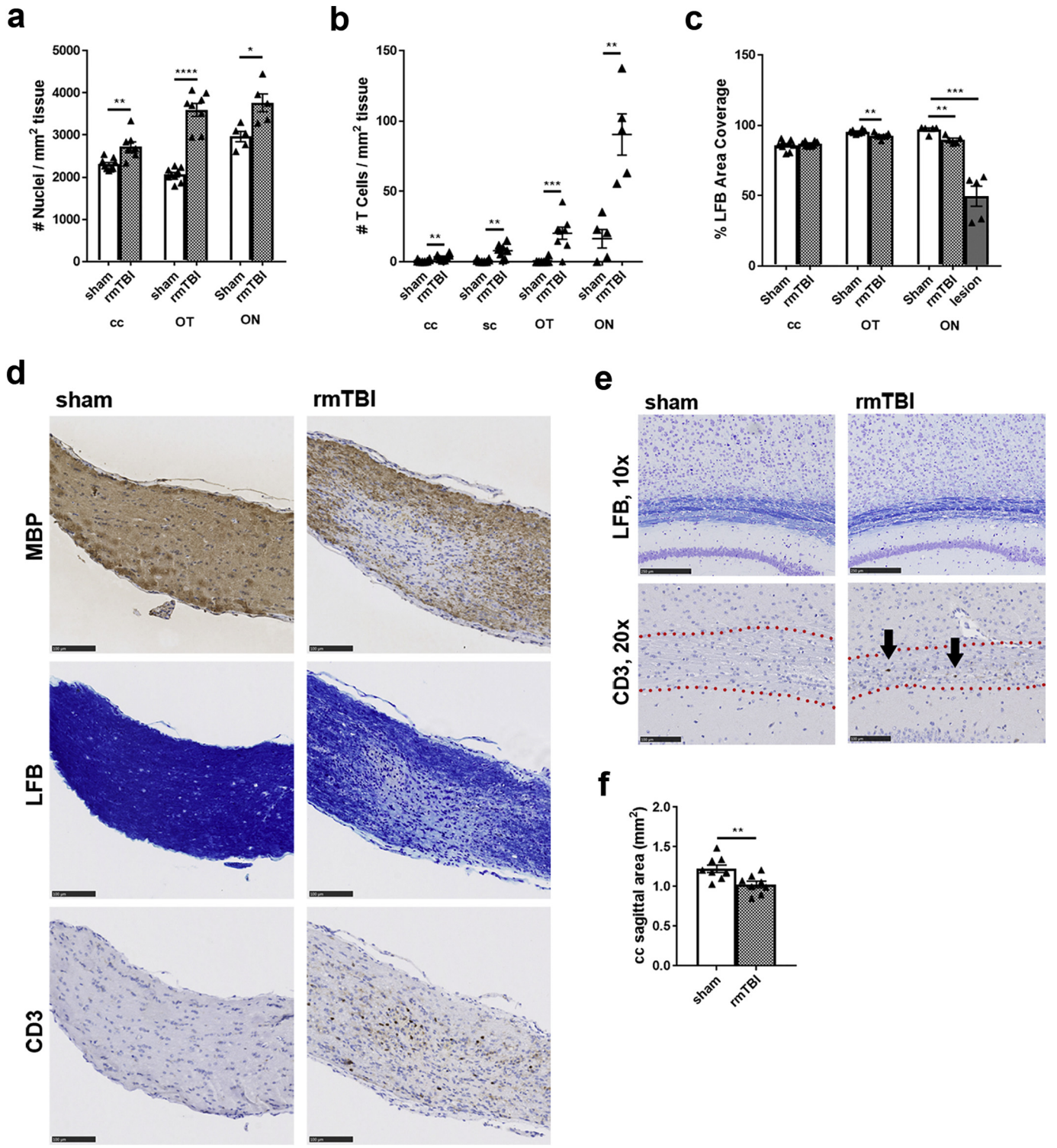

Fig. 4. T-cell infiltration and demyelination in white matter of injured Tau58.4 mice.
a) Quantification of white matter cellularity in cc, OT, and ON of Tau58.4 mice. b) Quantification of CD3 expressing T-cell counts per mm^2 tissue in cc, sc, OT, and ON. c) Quantification of myelin (LFB) coverage in cc, OT, ON, and ON lesions. d) Representative images of ON stained with MBP, LFB, and CD3. Staining in sc and OT is comparable to WT. Evident cavernous degeneration with increased cellularity in lesions can be observed. Scale bars, 100 μm. e) Representative image of cc stained with LFB and CD3. Note modest thinning of cc (highlighted in red dotted lines), with increased cellularity. Black arrows point to T-cells in cc. Scale bar, 10×: 250 μm; 20×: 100 μm. f) Quantification of cc sagittal area (mm^2) in sham vs injured Tau58.4 mice.
Bar graph and error bars indicate mean ± SEM. *p < 0.05; **p < 0.01; ***p < 0.001; ****p < 0.0001 vs sham by two-tailed Student's t-test.

differentially altered and sensitized by the Tau transgene. The genes selectively altered in Tau58.4 rmTBI mice over WT mice were enriched in pathways for protein modification, cellular response to stress, and apoptotic signaling (Suppl. Fig. 7a). Furthermore, when comparing differentially expressed gene sets caused by rmTBI in Tau and WT mice separately, additional downregulated pathways in axon/dendrite development and synapse organization were found to be enriched in Tau58.4 mice only (Suppl. Fig. 7b,c).

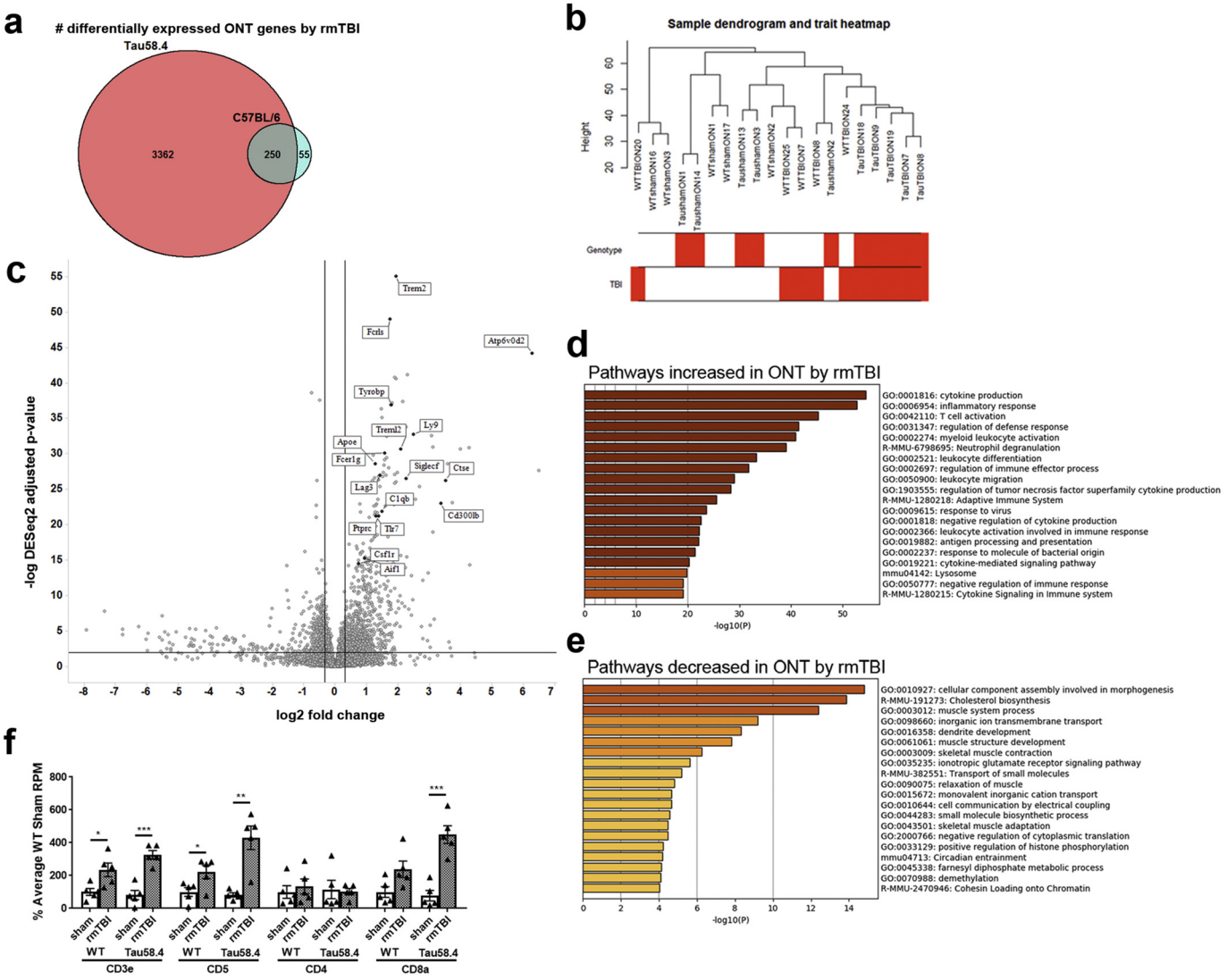

Fig. 5. Gene expression signatures of injured optic nerve and tract in both C57BL/6 and Tau58.4 mice.
a) Venn diagram of number of significantly changed genes vs respective shams in ONT of injured mice. $n = 5$/group/genotype. Significance was determined by DESeq2 adjusted p-value < 0.01. b) Hierarchal clustering by UPGMA of ONT samples with genotype and rmTBI status. Red genotype denotes Tau58.4 samples and red TBI status denotes rmTBI samples. c) Volcano plot of altered genes caused by rmTBI. Itgax, Cd22, and Cst7 were increased genes out of plot range. d) Metascape pathway analysis of all genes increased over 25% with adjusted p-value < 0.01. e) Metascape pathway analysis of all genes decreased by 25% or more with adjusted p-value < 0.01. f) Quantification of T-cell marker gene expression from the RNAseq dataset. Values were normalized to average RPM of WT sham mice.
Bar graph and error bars indicate mean ± SEM. $*p < 0.05$; $**p < 0.01$; $***p < 0.001$ vs respective sham by two-tailed Student's t-test.

3.4. rmTBI enhances astrocytic and microglial signatures, while decreasing oligodendrocytic and neuronal gene signatures in ONT of injured Tau mice

To further elucidate cell type responses to rmTBI in the ONT, gene signatures pulled from published single-cell and cell-type enriched RNAseq data (Zeisel et al., 2015; Zhang et al., 2014) were aligned to the current dataset. This revealed a differential cell type response which appears to be enhanced by the Tau transgene (Fig. 6a). Similar to what was seen by histology, astrocytic and myeloid signatures are generally increased by rmTBI. Closer examination of astrocyte signatures reveals an enrichment of pan-astrocyte and reactive "A1" astrocyte signatures (Liddelow et al., 2017), especially in Tau mice (Suppl. Fig. /8a). Conversely, the gene signatures of oligodendrocytes and neurons trend towards a decrease, which corroborates our observations of decreased LFB and increased FJC staining. This decrease is ambiguous in the WT animals. Because the gene expression data suggested neuronal signature loss, we stained injured ON from Tau58.4 mice for neuronal βIII-tubulin and confirmed loss of staining, with evidence of axonal swelling (Suppl. Fig. 8b).

To determine if there were differences in expression patterns associated with various stages of oligodendrocyte differentiation, we investigate the genes enriched in either oligodendrocyte progenitor cells (OPCs), newly formed oligodendrocytes, or myelinating oligodendrocytes (Zhang et al., 2014). Several OPC and newly formed oligodendrocyte signatures were revealed along with a more robust decrease in mature myelinating oligodendrocytes (Fig. 6b). This suggests that rmTBI results in a more selective loss of myelinating oligodendrocytes, with fewer alterations in OPCs.

Amongst these oligodendrocytic genes, Gpr17 and Gpr37 were significantly altered (adjusted p-value < .05) in both cortex and ONT by rmTBI. Gpr17 was increased while Gpr37 was decreased at 1mo in both tissues with both genotypes (Fig. 6c). Because Gpr17 and Gpr37 have links to demyelination and TBI (Chen et al., 2009; Lecca et al., 2008; Franke et al., 2013; Simon et al., 2015; Yang et al., 2016; Smith et al., 2017), we probed Mbp, Mog, Gpr37, and the Gpr17 signaling pathway (Chen et al., 2009; Fumagalli et al., 2011) at 3mo post-injury in ONT of

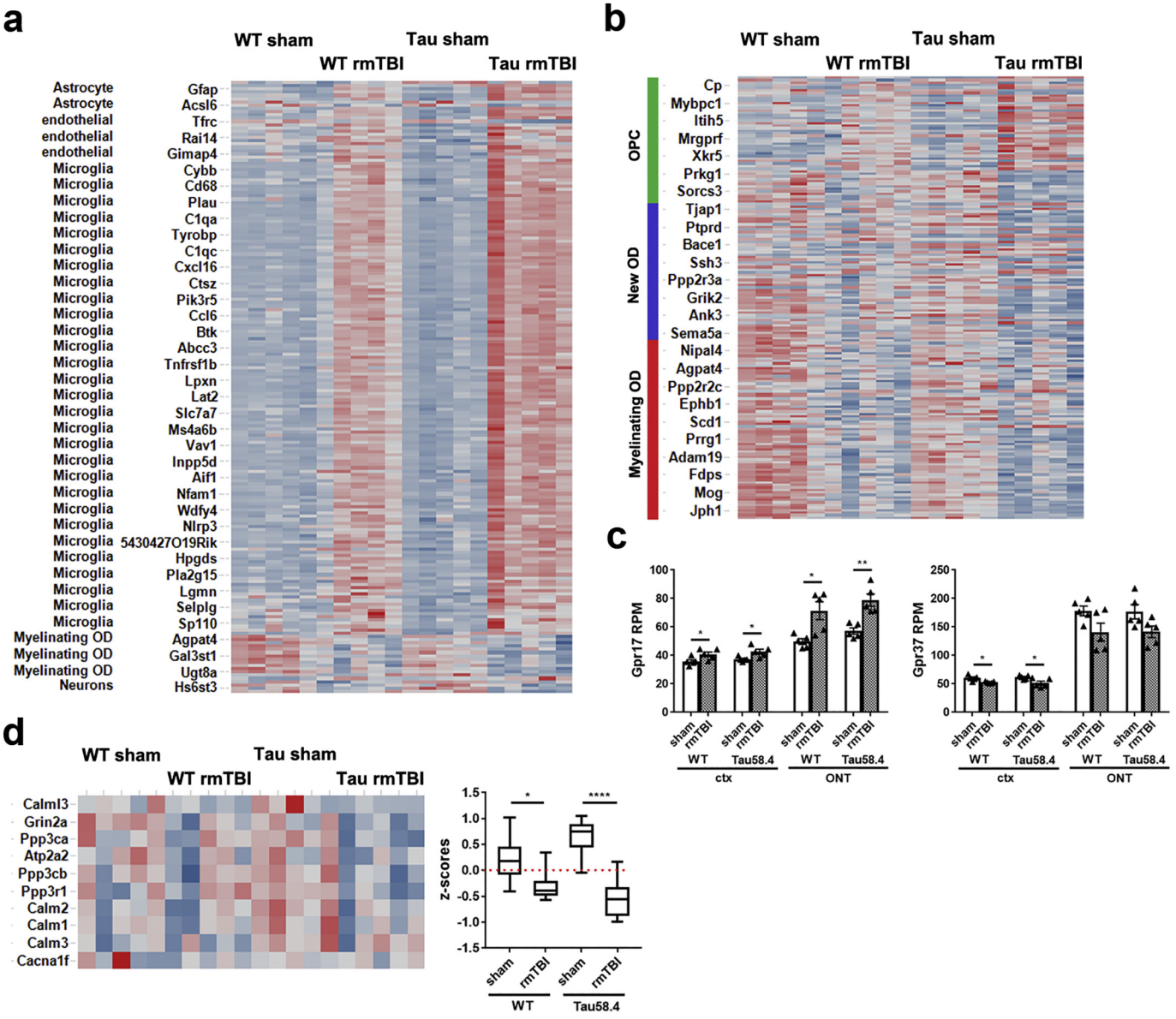

Fig. 6. Brain cell type-specific alterations in injured optic nerve and tract in C57BL/6 and Tau58.4 mice.
a) Heat map of differentially expressed astrocytic, endothelial, microglial (or myeloid), myelinating oligodendrocyte (OD), and neuronal enriched genes in ONT. Gene list was derived from cell type-specific signatures common to both Zeisel 2015 and Zhang 2014. Red indicates increase, blue indicates decrease compared to average z-score across all samples. $n = 5$/group/genotype. b) Heat map of differentially expressed oligodendrocyte lineage genes (gene list from Zhang et al. 2014) in ONT of injured mice. c) Quantification of Gpr17 and Gpr37 RPM from RNAseq dataset in ctx and ONT in WT and Tau58.4 mice. Bar graph and error bars indicate mean ± SEM. *$p < 0.05$; **$p < 0.01$ vs respective shams by two-tailed Student's *t*-test. d) Heat map of CTE progression genes identified in Seo et al. 2017 aligned to the ONT of the current data set. Box and whisker plot represents min-max quartiles consisting of average z-score per gene ($n = 10$ CTE progression genes) per group. *p < 0.05; ****$p < 0.0001$ vs respective shams by one-way ANOVA with Tukey post-test. (For interpretation of the references to color in this figure legend, the reader is referred to the web version of this article.)

WT and Tau58.4 mice. Mbp and Mog expression were unchanged in cortex and decreased 40–50% in ONT of both genotypes (Suppl. Fig. 9). In Tau58.4 mice, the only notable change was Id2, the Gpr17 downstream effector (Chen et al., 2009), which was significantly increased in both brain regions. In WT mice, Gpr37 was decreased in ONT, but Gpr17, Olig2, and Id2 were all unchanged in cortex and ONT (Suppl. Fig. 9). These genes could be useful markers of injury to supplement evidence for myelin loss.

3.5. rmTBI in mouse results in gene signatures that are observed in human neurodegenerative diseases

The gene expression changes in injured mouse ONT were compared to signatures of human AD and CTE brain to see if there were conserved mechanisms of neurodegeneration. We used published human AD cortical data from Zhang 2013 (Zhang et al., 2013) to represent human AD and Seo 2017 (Seo et al., 2017) represent human CTE. Many upregulated gene signatures in AD were also upregulated in the injured ONT of both Tau58.4 and WT mice (Suppl. Fig. 10a,b). These included pathways for inflammation, cell adhesion, and tissue remodeling. In contrast, downregulated gene signatures of AD were only present in injured Tau58.4 mice, not WT (Suppl. Fig. 10c). These common enriched downregulated pathways in AD and rmTBI were primarily associated with loss of neurons and synaptic function, corresponding with the pathways sensitized by the tau transgene (Suppl. Fig. 7c). This further suggests differential neuronal responses to rmTBI that are affected by

the tau transgene.

Furthermore, Seo et al. identified 10 downregulated genes related to tau phosphatases in human CTE that were hypothesized to be CTE progression genes (Seo et al., 2017). These genes were significantly downregulated by rmTBI in ONT of both WT and Tau58.4 mice, suggesting some overlap in the transcriptional signatures of our injury model to key CTE modules (Fig. 6d).

3.6. Myelination-promoting compounds activated OPC differentiation but did not repair histopathologic lesions

Since histology and gene expression analysis both implicate demyelination as a pathological feature of rmTBI, we wanted to determine whether induction of remyelination could alter the pathology in Tau58.4 mice. We tested GSK239512, a histamine receptor H3 (H3R) antagonist, because of its reported efficacy for remyelinating lesions in relapsing-remitting multiple sclerosis (Chen et al., 2017; Schwartzbach et al., 2017). To first demonstrate in vitro efficacy, OPCs treated with 10 μM GSK239512 demonstrated a 50% increase in MBP staining vs DMSO (Suppl. Fig. 11a), which signifies an ability to cause OPC differentiation into mature oligodendrocytes.

Oral dosing of GSK239512 (10mpk b.i.d. in 0.5%MC, 0.1%Tween 80) for 1mo, starting 3 days post-rmTBI, showed an increase in Mog gene expression vs rmTBI, and brought Mbp and Gpr37 expression in ONT to sham levels (Fig. 7a). However, GSK239512 treated mice showed no change in the presence of demyelinated ON lesions by histology (Fig. 7b,c). We also looked at OLIG2+ oligodendrocytes in the ON to determine if GSK239512 alters oligodendrocyte lineage proportions. Despite the increase in ON cellularity with rmTBI (Fig. 7d), OLIG2+ nuclei represented about 55% of total nuclei in all groups (Fig. 7e). Near the rmTBI lesions, however, there were proportionally fewer cells with OLIG2+ nuclei, which was increased by GSK239512 (Fig. 7e,f).

Additionally, GSK239512 had no effect on tauopathy, ON neuronal staining, or myeloid cell infiltration into the white matter when compared to the rmTBI+vehicle group (Suppl. Fig. 11b,c). In the brain, GSK239512 also failed to influence OT demyelination and did not influence myelin in the CC (Suppl. Fig. 11d). Consistent with the cortical RNAseq data, rmTBI caused a 30% reduction in Mog expression in the cortex vs sham, with no effect on Mbp. Treatment with GSK239512 increased cortex Mog to sham levels, but was not significantly different from rmTBI+vehicle groups (Suppl. Fig. 11e). Together, these data suggest H3R antagonists that induce OPC differentiation and remyelination are insufficient to repair white matter lesions caused by rmTBI, at least at the stage of disease modeled here.

3.7. Mice lacking T-cells show white matter neuroinflammation with fewer lesions

Due to the lack of remyelination efficacy with GSK239512 in vivo, we hypothesized that the chronic neuroinflammatory environment of monocytes, microglia, and/or T-cells in white matter tracts exacerbated

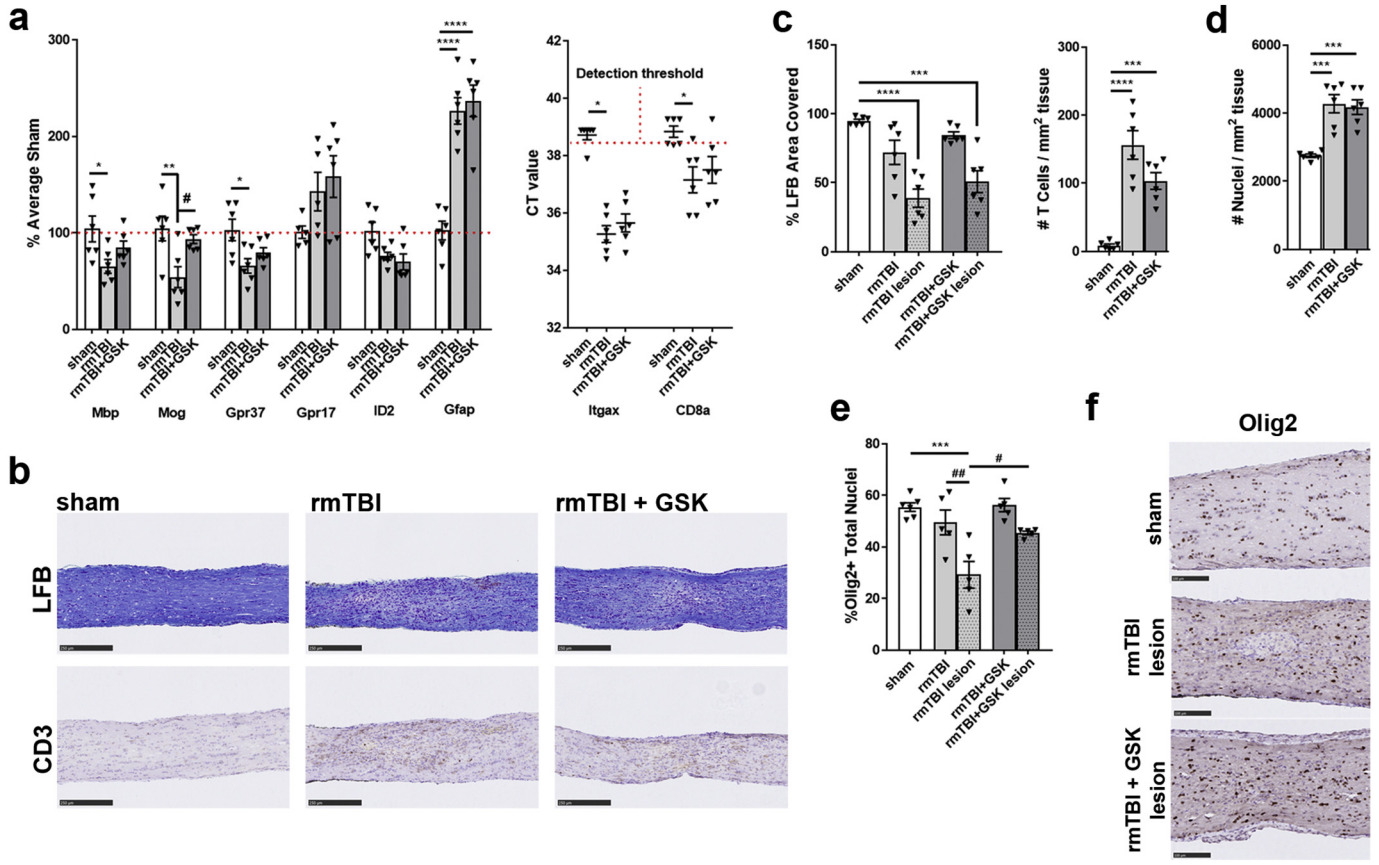

Fig. 7. Remyelination-inducing compound failed to repair demyelinated lesions of injured Tau58.4 mice.
a) Quantification of gene expression of several myelin related genes and inflammation genes by qPCR. Itgax and CD8a were plotted by CT values due to their low detection threshold, which leads to high variability when normalized to 36B4. $n = 6$/group. b) Representative images of ON stained with LFB and CD3 from sham, rmTBI, and rmTBI+GSK239512 (GSK) treated Tau58.4 mice. Scale bar: 250 μm. c) Quantification of LFB and CD3 staining data in the ON and ON lesions of sham, injured, and GSK treated mice. d) Quantification of cellularity in the ON. e) Quantification of the proportion of Olig2-positive nuclei in the ON across the whole nerve and around the lesions in rmTBI-exposed mice. f) Representative images of Olig2 staining in the ON with different conditions. Scale bar: 100 μm.
Bar graph and error bars indicate mean ± SEM. *$p < 0.05$; **$p < 0.01$; ***$p < 0.001$; ****$p < 0.0001$ vs shams. #p < .05; ##p < .01 vs rmTBI or rmTBI lesion. *P*-values generated by one-way ANOVA with Tukey post-test.

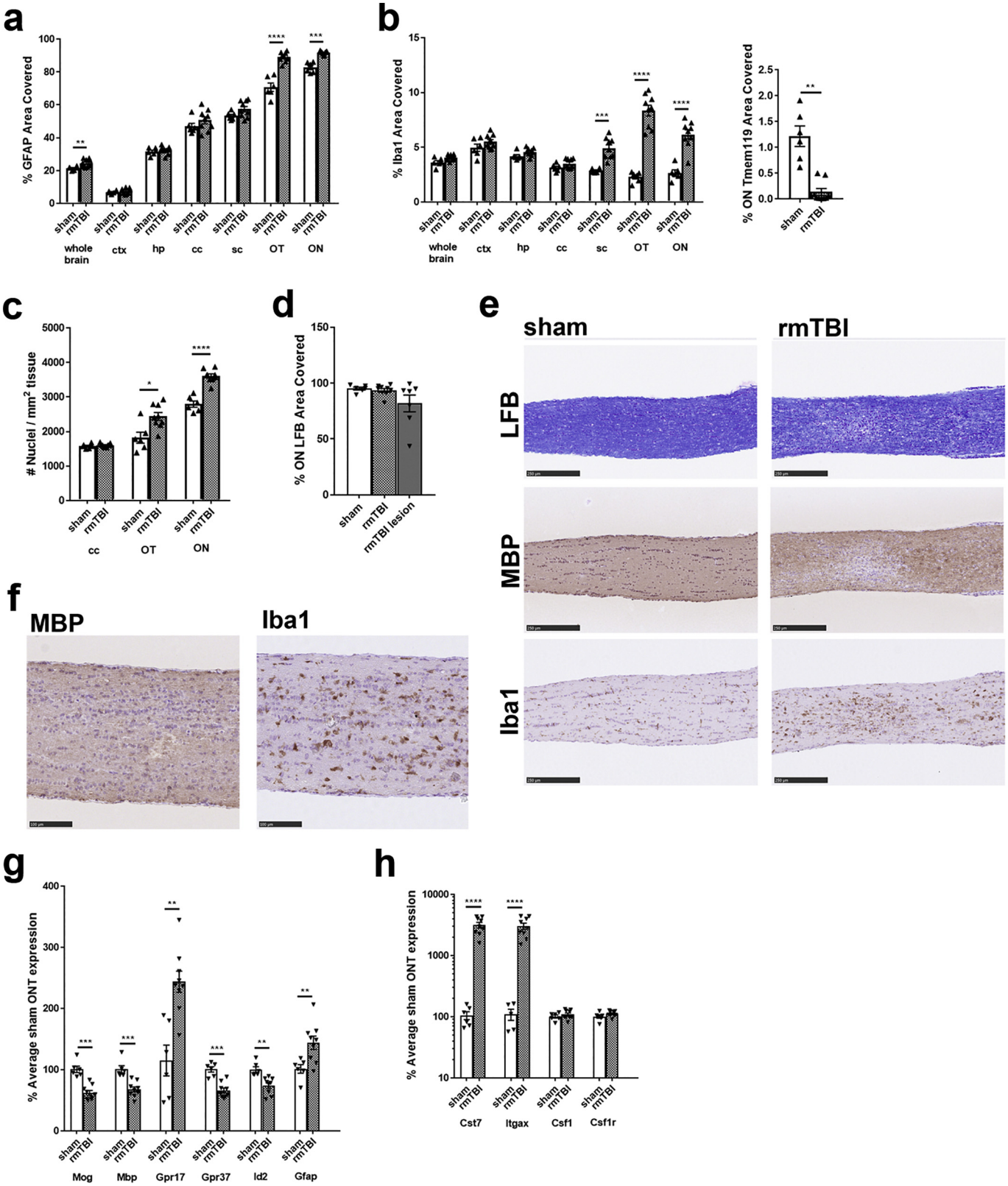

Fig. 8. R2G2 immune deficient mice show blunted optic nerve demyelination without affecting myeloid cell infiltration.
a) Quantification of GFAP in brain and ON in R2G2 mice. n = 6 sham, n = 9 rmTBI. b) Quantification of Iba1 in brain regions and ON Tmem119. c) Quantification of cellularity as nuclei counts/mm^2 in several white matter regions. d) Quantification of LFB myelin staining in ON and lesions in samples that showed evidence for lesions (n = 7). e) Representative images of LFB, MBP, and Iba1 staining in sham and rmTBI exposed R2G2 mice. Scale bar: 250 μm. f) Image of an inflammatory "lesion" without significant loss of MBP. Scale bar: 100 μm. g) Quantification of gene expression for myelin related genes and Gfap vs average sham levels. h) Quantification of gene expression for myeloid cell related genes.
Bar graph and error bars indicate mean ± SEM. *p < 0.05; **p < 0.01; ***p < 0.001; ****p < 0.0001 vs shams.

lesions and are prohibitive for repair. As T-cell activation was one of the most enriched GO terms by rmTBI, we utilized Rag2-Il2rg double knockout mice (R2G2), which lack lymphocytes (Shinkai et al., 1992), to test the role of T-cells in rmTBI-mediated lesion formation in the ON. We first confirmed the lack of lymphocytes and assessed the general leukocyte frequencies in R2G2 vs Tau58.4 mice by mass cytometry at 1mo post-injury. R2G2 mice show leukopenia as they only have 10% leukocyte counts vs Tau58.4 mice (Suppl. Fig. 12a). There was no effect of rmTBI on any peripheral leukocyte populations in R2G2 or in Tau58.4 mice (Suppl. Fig. 12b).

Despite the lack of T-cell lymphocytes, rmTBI still resulted in significant neuroinflammation of the ONT at 1mo with increases in Iba1-expressing myeloid cells, GFAP astrocytes, cellularity, and loss of Tmem119-expressing homeostatic microglia (Fig. 8a-c). However, there was not a significant loss of myelin by LFB and MBP staining (Fig. 8d,e). Distinct demyelinated lesions were only detected in ON of 2/9 R2G2 mice, while inflammatory lesions characterized by regions of disrupted nuclei and inflammatory cells were detected in 7/9 mice (Fig. 8d-f). Despite the attenuated myelin loss by histology, gene expression analysis of the ONT revealed similar patterns to what was observed in WT and Tau58.4 mice. The myelin-related genes Mog, Mbp, Gpr37, and Id2 were decreased by about 40%, while Gfap and Gpr17 were increased (Fig. 8g). Curiously, although myeloid cells were increased in the ON, Csf1, a cytokine, and Csf1r, a myeloid cell marker that was upregulated post-injury in both WT and Tau58.4 mice, were unchanged in injured R2G2 ONT compared to shams (Fig. 8h). This could indicate an alteration of myeloid cell signaling in R2G2 mice due to lack of lymphocytes. Overall, this data suggests that T-cells may contribute to chronic white matter injury and myeloid cell signaling during rmTBI.

4. Discussion

In this study, we explore a model of rmTBI that results in initial white matter inflammation, which progresses to chronic demyelination, neuroinflammation, and neurodegeneration with tau-overexpression. By performing histology and transcriptomic analysis on the white matter, we were able to identify interesting immune-related pathways and downregulated myelination, neurite development, and protein processing pathways associated with CTE. Our results demonstrate that a single impact is insufficient to induce chronic injury, and that human tau-overexpression exacerbates rmTBI pathology from 1mo to 3mo post-injury. The exacerbation of neuroinflammation has important implications for the brain's potential to repair damaged axons and white matter lesions (Kou and VandeVord, 2014).

Overall, these facets of our model share similarities to human CTE, where repetitive hits to the head are necessary for pathogenesis that results in chronic progressive neuroinflammation and degeneration over the span of decades. Several clinical studies on human concussion patients have used diffusion tensor imaging (DTI) to establish a link between impact-injury and acute white matter microstructural changes that correlate to behavioral alterations (Hellstrøm et al., 2017; Mustafi et al., 2018; Lancaster et al., 2018). These human studies of acute responses to mild TBI demonstrate that similarly to what was observed in our model, white matter tracts are amongst the earliest regions to be affected by injury and can contribute to CTE pathogenesis. Evidence from deceased CTE-diagnosed patients validate this claim, as even in Stage I CTE, clusters of reactive microglia are found in white matter with axonal swellings (McKee et al., 2015), comparable to what is seen in the CC and ONT of our mouse model. Evidence from early CTE cases suggests that pathology begins in the perivascular regions of the cerebral sulci, which can include both white and grey matter (Stein et al., 2014; McKee et al., 2015). While mice do not have comparable cerebral sulci, it is notable that our model shows neuroinflammation in the SC, which lies beneath the sulci-like transverse fissure. Pertinently, the white matter tracts of the SC and visual pathway are also affected in CTE (Armstrong, 2018; Armstrong et al., 2017), although this is likely due to widespread brain damage as opposed to a region-specific effect. Most importantly, CTE is defined by progressive neurodegeneration and inflammation of grey and white matter with accompanying increase of phosphor-tau burden (McKee et al., 2015). Although rmTBI did not induce or accelerate tauopathy in our model, it is clear that the human Tau transgene contributed to the progressive chronic outcomes of rmTBI. Thus, comparisons between WT and human Tau-overexpressing mice are useful to better bridge the understanding of how human Tau can contribute to disease pathogenesis and improve rodent model relevance.

Complementing our study with Tau-overexpressing mice, studies using Tau-knockouts have shown allelic dose-dependent protective trends for CC axonopathy following 2-hit rmTBI (Cheng et al., 2014). This comparison is important because rmTBI did not induce any tauopathy in WT mice, which could account for the relatively attenuated rmTBI histopathology. In the literature, there is inconsistency for rmTBI to induce tauopathy in rodents, especially in a C57BL/6 background (Yoshiyama et al., 2005; Mannix et al., 2013; Mouzon et al., 2014; Kalish and Whalen, 2016; Mouzon et al., 2017). Several studies have reported induction of phosphor-tau in rmTBI-exposed WT mice using the AT8 antibody utilized in the current study (Petraglia et al., 2014; Luo et al., 2014; Kondo et al., 2015). However, AT8 has been reported to have high non-specificity (Petry et al., 2014), so caution must be taken when making interpretations without cross-validation using other tau antibodies recognizing different epitopes. We cannot discount the possibility that our model may induce other epitopes of phosphorylated tau such as cis-P-tau, which is an early driver of neurodegeneration in rmTBI (Kondo et al., 2015). It is also notable that TBI models such as lateral fluid percussion have resulted in tauopathy and white matter injury in other mammalian species like rats and pigs (Tan et al., 2016; Wright et al., 2017; Smith et al., 1999). This adds confidence that white matter and axonal injury mechanisms manifest similarly amongst mammals but that tauopathy may vary between modelling species and injury type or severity. From this context, it is possible that our rmTBI in the current paradigm did not have sufficient biomechanics to induce tauopathy.

Notably, we have identified chronic myeloid and T-cell infiltration into the ONT that does not subside by 3mo. This is in contrast to microarray studies of a histopathologically similar optic nerve crush model where gene expression changes in the ON were largely attenuated by 3mo (Qu and Jakobs, 2013). While the role of microglia has been characterized in human CTE (Makinde et al., 2017; Cherry et al., 2016; Lucke-Wold et al., 2014; Coughlin et al., 2017), the role of peripheral macrophages and T-cells is unknown. A recent study reported a positive correlation between CD8 T-cell presence and human CTE progression with concomitant negative correlation with CC thickness (Huber et al., 2018). This would correspond with our gene expression detection of CD8 and evidence of CC thinning in ONT of injured Tau58.4 mice, adding a new angle to study CTE pathogenesis. Specifically, in injured mice, we observed many CD3 T-cells and Iba1-expressing myeloid cells in the choroid plexus, a known immune-brain gateway during neuroinflammation (Wilson et al., 2010; Schwartz and Baruch, 2014), adjacent to affected white matter tracts. We surmise that the initial injury leads to transient BBB impairment in the ONT that permits an influx of peripheral immune cells into the white matter. The injury may also activate the choroid plexus via cytokines such as Tnfα (Schwerk et al., 2010) that enables further transmigration of peripheral cells into the brain. This is supported by the transient increase in ON lesion IgG at 1d to 1mo post-rmTBI, followed by upregulated of cellular adhesion genes like vcam1, which are known to increase choroid plexus trafficking (Meeker et al., 2012).

Once in the injured ON, the infiltrating immune cells likely become tissue resident and may contribute to the increased detection of Ki67 + dividing cells and scarring. Rapid acceleration-deceleration shear forces such as those present in our TBI model will lead to diffuse axonal injury (Namjoshi et al., 2014; Xu et al., 2016; Evanson et al., 2018; Tzekov

et al., 2016), characterized by axonal beading and broken myelin fragments. These myelin fragments may be phagocytosed by microglia and macrophages over the course of Wallerian degeneration of the injured retinal ganglion axons in the ON (Hirata and Kawabuchi, 2002; Neumann et al., 2009; Kopper and Gensel, 2018). T-cells then may be activated by these microglia, macrophages, and other antigen presenting cells that are present at the lesion (Nizamutdinov and Shapiro, 2017; Schetters et al., 2018). While it is unclear whether the lesion-associated T-cells in our model are autoreactive to antigens like myelin, autoreactive T-cells to CNS antigens have been recovered from TBI patients (Cox et al., 2006). Similarly, in a model of ON crush, T cells were also found to accumulate in the injured ON regardless of antigenic specificity to MBP (Hirschberg et al., 1998). In this study, we saw evidence of CD8 T-cell gene expression at 1mo post-injury in both WT and Tau58.4 mice, which may reflect active cell killing (i.e. of oligodendrocytes and neurons) and exacerbated cytokine secretion leading to a positive feedback loop for more leukocyte infiltration. Furthermore, the observation that injured Tau58.4 mice had increased OPC gene signatures and decreased mature oligodendrocyte signatures suggests possible impairment of OPC differentiation or maturation at the lesion site due to the local cellular and inflammatory environment. It is also noteworthy that Tau58.4 mice had larger decreases in myelinating oligodendrocyte gene signatures than WT mice in the ONT, even at baseline. In fact, Tau58.4 mice have been reported to show hypomyelination in other white matter nerve tracts such as the sciatic nerve by 12mo of age (Yin et al., 2017). Although our data does not suggest hypomyelination in Tau58.4 vs WT shams at the age of sacrifice (~4-5mo), this age-dependent nerve hypomyelination in Tau58.4 mice could be a potential sensitizer to rmTBI damage. This mechanism of rmTBI-mediated injury is schematically summarized in Fig. 9.

In addition to alterations of oligodendroglia, there were also changes to glial homeostasis as we saw a loss of microglial TMEM119 and an increase of reactive astrocyte signatures in the ONT. Reactive "A1" astrocytes are neurotoxic and can be induced by microglial C1q, Tnfα, and Il1α (Liddelow et al., 2017). These factors were all increased in the injured Tau58.4, but not WT, ONT. This difference may contribute to the relative attenuation of responses in WT mice. The loss of TMEM119 staining in the injured ON lesions implies a conversion of homeostatic microglia into activated phagocytic microglia, and that the majority of Iba1-expressing cells have peripheral myeloid origins. This loss of TMEM119 around lesion sites has been described in demyelinating diseases such as MS (Zrzavy et al., 2017; Satoh et al., 2016). This is indicative of a local inflammatory environment that is damaging to neuronal survival and repair.

While rmTBI in both WT and Tau58.4 mice resulted in upregulation of inflammatory signatures and downregulation of cholesterol biosynthesis signatures, only Tau58.4 mice showed downregulated signatures of axonogenesis, synapse organization, and dendrite development pathways (Suppl. Fig. 7). Additionally, because Tau58.4 mice will naturally develop progressive tauopathy with concomitant neuroinflammation (van Eersel et al., 2015), there are different baseline effects at play that may alter rmTBI responses. However, even after controlling for these differences in baseline, Tau58.4 mice show exacerbated and progressive inflammation across both white matter and grey matter after rmTBI that is not observed in WT mice (Supp Figs. 2 & 5). Thus, we hypothesize that there are fundamental differences in the neurites with human P301S Tau mutation that make them more susceptible to traumatic axonal injury and cellular stress after rmTBI, which can lead to more axonal swelling, myelin debris, apoptosis, and an exacerbated inflammatory response. The ensuing deposition of phosphor-tau positive neurons in the cortex or hippocampus are also more sensitive to injury and activate local microglia, which eventually leads to a chronic neuroinflammatory and neurodegenerative state. These factors are not present in WT mice, hence the attenuated response.

To further demonstrate human relevance, we compared differentially expressed genes in our study to published data of human AD and CTE. The most important differences between our data and human patient data are the species and tissues compared. Our reference human transcriptomic studies have been conducted primarily in cortical tissue, with large variabilities in sample age and number of concussions

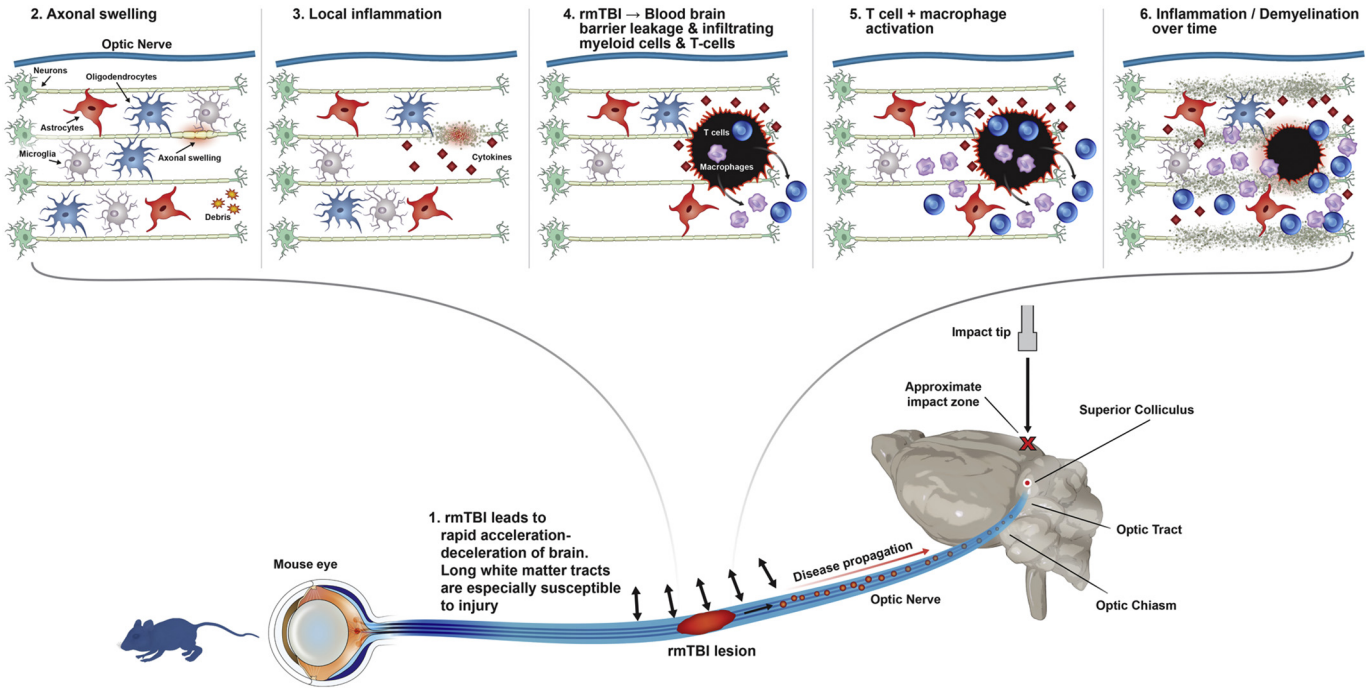

Fig. 9. Schematic summary of rmTBI mediated white matter damage.
rmTBI can lead to acute injury described in steps 1–4, where shear forces damage axons and myelin in white matter tracts such as the ONT. Impacts to the top of the head could lead to more exacerbated movement and injury of the ON due to its anatomical location under the brain. Many infiltrating cells become resident and continue to propagate inflammatory signaling and injury, leading to chronic inflammation, degeneration and demyelination over time (shown in steps 5–6). Tau58.4 mice are more prone to these processes.

experienced (Zhang et al., 2013; Seo et al., 2017). Despite these important distinctions, we saw associations with AD in our dataset, driven by changes in immune and adhesion-related gene pathways. While we did not see the same degree of association of our data to human CTE, human brains are gyrencephalic with many folds, while mouse brains are lissencephalic without folds. The presence of gyri and sulci in human brains is hypothesized to play a major role in development of CTE, as experimental and computational models suggest that brain sulcal depths are most vulnerable to the biomechanics of TBI events (McKee et al., 2015; Kornguth et al., 2017). Despite this, our data show similarities to key CTE module hubs where tauopathy sensitizes rmTBI damage through alterations of protein processing (Suppl. Fig). Tau phosphatases such as calcineurin-associated Ppp3ca were consistently decreased with rmTBI in Tau58.4 mice and may reflect similar pathology. Of interest, these protein phosphatases are also associated with neurofibrillary tangle formation and AD progression (Braithwaite et al., 2013). Overall, our data show important overlaps with human neurodegenerative disease.

Based on the model characterization findings, we attempted to modulate pathology by inducing remyelination and by genetic-based immunosuppression. We tested an H3R antagonist for remyelination because it had shown some efficacy in human MS trials (Schwartzbach et al., 2017) and reduced tauopathy in a transgenic mouse model following chronic dosing (Delay-Goyet et al., 2016). Despite this, our data showed no evidence that 1mo oral dosing of GSK239512 altered the course of tauopathy, which could be due to the relative short timeframe of treatment. In addition, GSK239512 showed no effect on improving myelination, inflammation, and axonal degeneration despite increasing OLIG2+ cell counts at lesions and restoring Mbp + Mog gene expression to sham levels in the ONT (Fig. 7a,e). This suggests that GSK239512 may promote OPC differentiation into MBP-expressing oligodendrocytes across the ONT, but not at the lesion. However, there is also the possibility that axonal degeneration is too severe and that there is insufficient material to remyelinate by the time compound dosing begins.

Finally, from our histology and expression profiling data, we hypothesized that T-cells may play a significant role in traumatic demyelination and the failure of lesion remyelination. Literature reports of T-cell deficient mice undergoing different models of TBI have shown contrasting results from protection to exacerbation to no effect (Gold et al., 2018; Alonso-Escalante et al., 2017; Weckbach et al., 2012). While our data suggests that T-cells do not significantly affect neuropathology, the attenuated Csf1r induction in injured R2G2 mice is interesting because it suggests that T-cells may play a role in secreting cytokines like Csf1 that can promote myeloid cell survival and activation (Zisman et al., 1993). In an immune-competent mouse, the T-cells that become resident after injury may signal to these infiltrating myeloid cells and macrophages for chronic recruitment and continued phagocytosis of myelin debris and cells, which leads to larger demyelinated lesions over time (Suppl. Fig. 5e). This dynamic may account for the attenuation of demyelinated lesions in injured R2G2 mice at 1mo.

There are several limitations and caveats to our study. Most importantly in mice, 1-3mo post-injury as assessed in the current study is a relatively short timeframe compared to the decades CTE takes to develop in humans. No conclusions can be made as to whether tauopathy may develop or accelerate at later time points. Regardless, our model should be viewed as an effective tool to better understand the pathogenesis of chronic rmTBI diseases such as CTE. Additionally, a common observation in other comparable rmTBI models that was not observed here is the presence of CC damage for WT mice (Petraglia et al., 2014; Ojo et al., 2016; Tagge et al., 2018; Namjoshi et al., 2014). We suspect our model is milder as we do not anesthetize and stabilize the mice head in ear bars prior to impacts. The ear bars may prevent the head from moving during impact and increase the pressure felt by the brain, leading to more severe injury. We also cannot discount the possibility that tools such as MRI or diffusion tensor imaging may be able to detect subtle changes in CC that we were unable to detect in WT mice via histopathology. Lastly, an important limitation of the current study is the lack of behavioral testing. Behavioral testing is an important functional readout for TBI models and can provide insights to subtle memory, cognitive, and motor deficits that may be applicable to how humans develop neurobehavioral issues post-TBI. Future studies are needed to document the neurobehavioral sequalae of disease in our model.

5. Conclusions

We have a developed a simple-to-execute, reproducible rodent model of rmTBI that argues for the usage of human Tau transgenic mice in future studies for their increased relevance to human CTE. While rmTBI resulted in white matter damage and demyelination in all models tested, only Tau58.4 mice showed evidence for progressive neuroinflammation, neuronal loss, and grey matter damage, which are all key components of human CTE. Ultimately, this study provides a useful model in which therapeutic modalities can be tested to help identify possible pathways that can improve CTE outcomes, especially concerning white matter damage. Future studies will be conducted to study the alterations of neuronal responses in Tau58.4 mice, with emphasis on neuroprotection post-rmTBI and resolution of chronic neuroinflammation.

Declaration of Competing Interest

All authors are employees of Novartis, some whom may hold company stock.

Acknowledgements

This work was funded by the Novartis Institute for Biomedical Research and The Genomics Institute for the Novartis Research Foundation's postdoctoral program.

Appendix A. Supplementary data

Supplementary data to this article can be found online at https://doi.org/10.1016/j.nbd.2019.104683.

References

Acabchuk, R., Briggs, D.I., Angoa-Pérez, M., Powers, M., Wolferz Jr., R., Soloway, M., et al., 2016. Repeated mild traumatic brain injury causes focal response in lateral septum and hippocampus. Concussion 1 (3). https://doi.org/10.2217/cnc-2015-0001.

Alhilali, L.M., Delic, J.A., Gumus, S., Fakhran, S., 2015. Evaluation of white matter injury patterns underlying neuropsychiatric symptoms after mild traumatic brain injury. Radiology 277, 793–800. https://doi.org/10.1148/radiol.2015142974.

Alonso-Escalante, J.C., Hamade, D.F., Sodhi, C.P., Fulton, W., Hackam, D.J., Nasr, I.W., 2017. The role of the innate and adaptive immune Systems in the Pathogenesis of traumatic brain injury in mice. Acad. Surg. Congress 3, 6.

Alosco, M.L., Koerte, I.K., Tripodis, Y., Mariani, M., Chua, A.S., Jarnagin, J., et al., 2017. White matter signal abnormalities in former National Football League players. Alzheimers Dement. 10, 56–65. https://doi.org/10.1016/j.dadm.2017.10.003.

Andorfer, C., Kress, Y., Espinoza, M., de Silva, R., Tucker, K.L., Barde, Y.A., et al., 2003. Hyperphosphorylation and aggregation of tau in mice expressing normal human tau isoforms. J. Neurochem. 86, 582–590.

Armstrong, R.A., 2018. Visual problems associated with traumatic brain injury. Clin. Exp. Optom 101, 716–726. https://doi.org/10.1111/cxo.12670.

Armstrong, R.A., McKee, A.C., Cairns, N.J., 2017. Pathology of the superior colliculus in chronic traumatic encephalopathy. Optom. Vis. Sci. 94, 33–42. https://doi.org/10.1097/OPX.0000000000000911.

Bai, R., Gao, H., Han, Z., Huang, S., Ge, X., Chen, F., et al., 2017. Flow cytometric characterization of T cell subsets and microglia after repetitive mild traumatic brain injury in rats. Neurochem. Res. 42, 2892–2901. https://doi.org/10.1007/s11064-017-2310-0.

Baugh, C.M., Stamm, J.M., Riley, D.O., Gavett, B.E., Shenton, M.E., Lin, A., et al., 2012. Chronic traumatic encephalopathy: neurodegeneration following repetitive concussive and subconcussive brain trauma. Brain Imaging Behav. 6, 244–254. https://doi.org/10.1007/s11682-012-9164-5.

Bennett, M.L., Bennett, F.C., Liddelow, S.A., Ajami, B., Zamanian, J.L., Fernhoff, N.B., et al., 2016. New tools for studying microglia in the mouse and human CNS. Proc. Natl. Acad. Sci. 113, E1738–E1746. https://doi.org/10.1073/pnas.1525528113.

Braithwaite, S.P., Stock, J.B., Lombroso, P.J., Nairn, A.C., 2013. Protein phosphatases and Alzheimer's disease. Prog. Mol. Biol. Transl. Sci. 106343–106379. https://doi.org/10.1016/B978-0-12-396456-4.00012-2.

Briggs, D.I., Angoa-Pérez, M., Kuhn, D.M., 2016. Prolonged repetitive head trauma induces a singular chronic traumatic encephalopathy-like pathology in white matter despite transient behavioral abnormalities. Am. J. Pathol. 186, 2869–2886. https://doi.org/10.1016/j.ajpath.2016.07.013.

Chen, Y., Wu, H., Wang, S., Koito, H., Li, J., Ye, F., et al., 2009. The oligodendrocyte-specific G protein-coupled receptor GPR17 is a cell-intrinsic timer of myelination. Nat. Neurosci. 12, 1398–1406. https://doi.org/10.1038/nn.2410.

Chen, Y., Zhen, W., Guo, T., Zhao, Y., Liu, A., Rubio, J.P., et al., 2017. Histamine receptor 3 negatively regulates oligodendrocyte differentiation and remyelination. PLoS One 12, e0189380. https://doi.org/10.1371/journal.pone.0189380.

Cheng, J.S., Craft, R., Yu, G.Q., Ho, K., Wang, X., Mohan, G., et al., 2014. Tau reduction diminishes spatial learning and memory deficits after mild repetitive traumatic brain injury in mice. PLoS One 9 (12). https://doi.org/10.1371/journal.pone.0115765.

Cherry, J.D., Tripodis, Y., Alvarez, V.E., Huber, B., Kiernan, P.T., Daneshvar, D.H., 2016. Microglial neuroinflammation contributes to tau accumulation in chronic traumatic encephalopathy. Acta Neuropathol. Commun. 4, 112. https://doi.org/10.1186/s40478-016-0382-8.

Coughlin, J.M., Wang, Y., Minn, I., Bienko, N., Ambinder, E.B., Xu, X., 2017. Imaging of glial cell activation and white matter integrity in brains of active and recently retired National Football League Players. JAMA Neurol. 74, 67–74. https://doi.org/10.1001/jamaneurol.2016.3764.

Cox, A.L., Coles, A.J., Nortje, J., Bradley, P.G., Chatfield, D.A., Thompson, S.J., et al., 2006. An investigation of auto-reactivity after head injury. J. Neuroimmunol. 174, 180–186. https://doi.org/10.1016/j.jneuroim.2006.01.007.

Delay-Goyet, P., Blanchard, V., Schussler, N., Lopez-Grancha, M., Ménager, J., Mary, V., et al., 2016. SAR110894, a potent histamine H3-receptor antagonist, displays disease-modifying activity in a transgenic mouse model of tauopathy. Alzheimers Dement. 2, 267–280. https://doi.org/10.1016/j.trci.2016.10.002.

Evanson, N.K., Guilhaume-Correa, F., Herman, J.P., Goodman, M.D., 2018. Optic tract injury after closed head traumatic brain injury in mice: a model of indirect traumatic optic neuropathy. PLoS One 13 (5). https://doi.org/10.1371/journal.pone.0197346.

Franke, H., Parravicini, C., Lecca, D., Zanier, E.R., Heine, C., Bremicker, K., et al., 2013. Changes of the GPR17 receptor, a new target for neurorepair. In: Neurons and Glial Cells in Patients with Traumatic Brain Injury, https://doi.org/10.1007/s11302-013-9366-3.

Fumagalli, M., Daniele, S., Lecca, D., Lee, P.R., Parravicini, C., Fields, R.D., 2011. Phenotypic changes, signaling pathway, and functional correlates of GPR17-expressing neural precursor cells during oligodendrocyte differentiation. J. Biol. Chem. 286, 10593–10604. https://doi.org/10.1074/jbc.M110.162867.

Galgano, M., Russell, T., McGillis, S., Toshkezi, G., Chin, L., Zhao, L.R., 2015. A review of traumatic brain injury animal models: are we lacking adequate models replicating chronic traumatic encephalopathy? J. Neurol. Neurobiol. 2 (1). https://doi.org/10.16966/2379- 7150.117.

Gendron, T.F., Petrucelli, L., 2009. The role of tau in neurodegeneration. Mol. Neurodegener. 4, 13. https://doi.org/10.1186/1750-1326-4-13.

Giunta, B., Obregon, D., Velisetty, R., Sanberg, P.R., Borlongan, C.V., Tan, J., 2012. The immunology of traumatic brain injury: a prime target for Alzheimer's disease prevention. J. Neuroinflammation 9, 185. https://doi.org/10.1186/1742-2094-9-185.

Gold, E.M., Vasilevko, V., Hasselmann, J., Tiefenthaler, C., Hoa, D., Ranawaka, K., et al., 2018. Repeated mild closed head injuries induce long-term white matter pathology and neuronal loss that are correlated with behavioral deficits. ASN Neurol. 10https://doi.org/10.1177/1759091418781921. 1759091418781921.

Hellstrøm, T., Westlye, L.T., Kaufmann, T., Trung Doan, N., Søberg, H.L., Sigurdardottir, S., et al., 2017. White matter microstructure is associated with functional, cognitive and emotional symptoms 12 months after mild traumatic brain injury. Sci. Rep. 7, 13795. https://doi.org/10.1038/s41598-017-13628-1.

Hirata, K., Kawabuchi, M., 2002. Myelin phagocytosis by macrophages and non-macrophages during Wallerian degeneration. Microsc. Res. Tech. 57, 541–547. https://doi.org/10.1002/jemt.10108.

Hirschberg, D.L., Moalem, G., He, J., Mor, F., Cohen, I.R., Schwartz, M., 1998. Accumulation of passively transferred primed T cells independently of their antigen specificity following central nervous system trauma. J. Neuroimmunol. 89, 88–96.

Holleran, L., Kim, J.H., Gangolli, M., Stein, T., Alvarez, V., McKee, A., et al., 2017. Acta Neuropathol. 133, 367–380. https://doi.org/10.1007/s00401-017-1686-x.

Huber, B.R., Mahar, I., Kwasnik, D., Mathias, R., Alvarez, V., Cherry, J., et al., 2018. CD8-expressing cell density is stage-specifically increased in chronic traumatic encephalopathy and comorbid Alzheimer's disease. In: Society for Neuroscience 2018 Meeting. 565. pp. 10.

Johnson, V.E., Stewart, W., Smith, D.H., 2013. Axonal pathology in traumatic brain injury. Exp. Neurol. 246, 35–43. https://doi.org/10.1016/j.expneurol.2012.01.013.

Kalish, B.T., Whalen, M.J., 2016. Weight drop models in traumatic brain injury. Methods Mol. Biol. 1462, 193–209. https://doi.org/10.1007/978-1-4939-3816-2_12.

Kondo, A., Shahpasand, K., Mannix, R., Qiu, J., Moncaster, J., Chen, C.H., et al., 2015. Antibody against early driver of neurodegeneration cis P-tau blocks brain injury and tauopathy. Nature 523, 431–436. https://doi.org/10.1038/nature14658.

Kopper, T.J., Gensel, J.C., 2018. Myelin as an inflammatory mediator: myelin interactions with complement, macrophages, and microglia in spinal cord injury. J. Neurosci. Res. 96, 969–977. https://doi.org/10.1002/jnr.24114.

Kornguth, S., Rutledge, N., Perlaza, G., Bray, J., Hardin, A., 2017. A proposed mechanism for development of CTE following concussive events: head impact, water hammer injury, neurofilament release, and autoimmune processes. Brain Sci. 7, E164. https://doi.org/10.3390/brainsci7120164.

Kou, Z., VandeVord, P.J., 2014. Traumatic white matter injury and glial activation: from basic science to clinics. Glia 62, 1831–1855. https://doi.org/10.1002/glia.22690.

Lancaster, M.A., Meier, T.B., Olson, D.V., McCrea, M.A., Nelson, L.D., Muftuler, L.T., 2018. Chronic differences in white matter integrity following sport-related concussion as measured by diffusion MRI: 6-month follow-up. Hum. Brain Mapp. 39, 4276–4289. https://doi.org/10.1002/hbm.24245.

Laurer, H.L., Bareyre, F.M., Lee, V.M., Trojanowski, J.Q., Longhi, L., Hoover, R., et al., 2001. Mild head injury increasing the brain's vulnerability to a second concussive impact. J. Neurosurg. 95, 859–870. https://doi.org/10.3171/jns.2001.95.5.0859.

Lecca, D., Trincavelli, M.L., Gelosa, P., Sironi, L., Ciana, P., Fumagalli, M., et al., 2008. The recently identified P2Y-like receptor GPR17 is a sensor of brain damage and a new target for brain repair. PLoS One 3 (10). https://doi.org/10.1371/journal.pone.0003579.

Liddelow, S.A., Guttenplan, K.A., Clarke, L.E., Bennett, F.C., Bohlen, C.J., Schirmer, L., et al., 2017. Neurotoxic reactive astrocytes are induced by activated microglia. Nature 541, 481–487. https://doi.org/10.1038/nature21029.

Lucke-Wold, B.P., Turner, R.C., Logsdon, A.F., Bailes, J.E., Huber, J.D., Rosen, C.L., 2014. Linking traumatic brain injury to chronic traumatic encephalopathy: identification of potential mechanisms leading to neurofibrillary tangle development. J. Neurotrauma 31, 1129–1138. https://doi.org/10.1089/neu.2013.3303.

Luo, J., Nguyen, A., Villeda, S., Zhang, H., Ding, Z., Lindsey, D., et al., 2014. Long-term cognitive impairments and pathological alterations in a mouse model of repetitive mild traumatic brain injury. Front. Neurol. 5, 12. https://doi.org/10.3389/fneur.2014.00012.

Makinde, H.M., Just, T.B., Cuda, C.M., Perlman, H., Schwulst, S.J., 2017. The role of microglia in the etiology and evolution of chronic traumatic encephalopathy. Shock 48, 276–283. https://doi.org/10.1097/SHK.0000000000000859.

Mannix, R., Meehan, W.P., Mandeville, J., Grant, P.E., Gray, T., Berglass, J., 2013. Clinical correlates in an experimental model of repetitive mild brain injury. Ann. Neurol. 74, 65–75. https://doi.org/10.1002/ana.23858.

McKee, C.A., Lukens, J.R., 2016. Emerging roles for the immune system in traumatic brain injury. Front. Immunol. 7, 556. https://doi.org/10.3389/fimmu.2016.00556.

McKee, A.C., Stein, T.D., Kiernan, P.T., Alvarez, V.E., 2015. The neuropathology of chronic traumatic encephalopathy. Brain Pathol. 25, 350–364. https://doi.org/10.1111/bpa.12248.

Meeker, R.B., Williams, K., Killebrew, D.A., Hudson, L.C., 2012. Cell trafficking through the choroid plexus. Cell Adhes. Migr. 6, 390–396. https://doi.org/10.4161/cam.21054.

Mouzon, B.C., Bachmeier, C., Ferro, A., Ojo, J.O., Crynen, G., Acker, C.M., 2014. Chronic neuropathological and neurobehavioral changes in a repetitive mild traumatic brain injury model. Ann. Neurol. 75, 241–254. https://doi.org/10.1002/ana.24064.

Mouzon, B.C., Bachmeier, C., Ojo, J.O., Acker, C.M., Fergusen, S., Paris, D., et al., 2017. Lifelong behavioral and neuropathological consequences of repetitive mild traumatic brain injury. Ann. Clin. Transl. Neurol. 5, 64–80. https://doi.org/10.1002/acn3.510.

Multani, N., Goswami, R., Khodadadi, M., Ebraheem, A., Davis, K.D., Tator, C.H., et al., 2016. He association between white-matter tract abnormalities, and neuropsychiatric and cognitive symptoms in retired professional football players with multiple concussions. J. Neurol. 263, 1332–1341. https://doi.org/10.1007/s00415-016-8141-0.

Mustafi, S.M., Harezlak, J., Koch, K.M., Nencka, A.S., Meier, T.B., West, J.D., et al., 2018. Acute white-matter abnormalities in sports-related concussion: a diffusion tensor imaging study from the NCAA-DoD CARE consortium. J. Neurotrauma 35, 2653–2664. https://doi.org/10.1089/neu.2017.5158.

Namjoshi, D.R., Cheng, W.H., McInnes, K.A., Martens, K.M., Carr, M., Wilkinson, A., et al., 2014. Merging pathology with biomechanics using CHIMERA (Closed-Head Impact Model of Engineered Rotational Acceleration): a novel, surgery-free model of traumatic brain injury. Mol. Neurodegener. 9, 55. https://doi.org/10.1186/1750-1326-9-55.

Nemetz, P.N., Leibson, C., Naessens, J.M., Beard, M., Kokmen, E., Annegers, J.F., et al., 1999. Traumatic brain injury and time to onset of Alzheimer's disease: a population-based study. Am. J. Epidemiol. 149, 32–40.

Neumann, H., Kotter, M.R., Franklin, R.J., 2009. Debris clearance by microglia: an essential link between degeneration and regeneration. Brain 132, 288–295. https://doi.org/10.1093/brain/awn109.

Nizamutdinov, D., Shapiro, L.A., 2017. Overview of traumatic brain injury: an immunological context. Brain Sci. 7, 11. https://doi.org/10.3390/brainsci7010011.

Ojo, J.O., Mouzon, B.C., Crawford, F.F., 2016. Repetitive head trauma, chronic traumatic encephalopathy and tau: challenges in translating from mice to men. Exp. Neurol. 3, 389–404. https://doi.org/10.1016/j.expneurol.2015.06.003.

Omalu, B.I., DeKosky, S.T., Minster, R.L., Kamboh, M.I., Hamilton, R.L., Wecht, C.H., 2005. Chronic traumatic encephalopathy in a National Football League player. Neurosurgery 128:128–134.

Petraglia, A.L., Plog, B.A., Dayawansa, S., Dashnaw, M.L., Czerniecka, K., Walker, C.T., 2014. The pathophysiology underlying repetitive mild traumatic brain injury in a novel mouse model of chronic traumatic encephalopathy. Surg. Neurol. Int. 5, 184. https://doi.org/10.4103/2152-7806.147566.

Petry, F.R., Pelletier, J., Bretteville, A., Morin, F., Calon, F., Hébert, S.S., et al., 2014. Specificity of anti-tau antibodies when analyzing mice models of Alzheimer's disease: problems and solutions. PLoS One 9, e94251. https://doi.org/10.1371/journal.pone.0094251.

Qu, J., Jakobs, T.C., 2013. The time course of gene expression during reactive gliosis in the optic Nerve. PLoS One 8, e67094. https://doi.org/10.1371/journal.pone.0067094.

Saher, G., Strumpf, S.K., 2015. Cholesterol in myelin biogenesis and hypomyelinating disorders. Biochim. Biophys. Acta 1851, 1083–1094. https://doi.org/10.1016/j.

bbalip.2015.02.010.
Satoh, J., Kino, Y., Asahina, N., Takitani, M., Miyoshi, J., Ishida, T., 2016. TMEM119 marks a subset of microglia in the human brain. Neuropathology 36, 39–49. https://doi.org/10.1111/neup.12235.
Schetters, S.T.T., Gomez-Nicola, D., Garcia-Vallejo, J.J., Van Kooyk, Y., 2018. Neuroinflammation: microglia and T cells get ready to tango. Front. Immunol. 8, 1905. https://doi.org/10.3389/fimmu.2017.01905.
Schwartz, M., Baruch, K., 2014. The resolution of neuroinflammation in neurodegeneration: leukocyte recruitment via the choroid plexus. EMBO J. 33, 7–22. https://doi.org/10.1002/embj.201386609.
Schwartzbach, C.J., Grove, R.A., Brown, R., Tompson, D., Then Bergh, F., Arnold, D.L., 2017. Lesion remyelinating activity of GSK239512 versus placebo in patients with relapsing-remitting multiple sclerosis: a randomised, single-blind, phase II study. J. Neurol. 264, 304–315. https://doi.org/10.1007/s00415-016-8341-7.
Schwerk, C., Rybarczyk, K., Essmann, F., Seibt, A., Mölleken, M.L., Zeni, P., 2010. TNFalpha induces choroid plexus epithelial cell barrier alterations by apoptotic and nonapoptotic mechanisms. J. Biomed. Biotechnol. 2010, 307231. https://doi.org/10.1155/2010/307231.
Seo, J.S., Lee, S., Shin, J.Y., Hwang, Y.J., Cho, H., Yoo, S.K., 2017. Transcriptome analyses of chronic traumatic encephalopathy show alterations in protein phosphatase expression associated with tauopathy. Exp. Mol. Med. 49, e333. https://doi.org/10.1038/emm.2017.56.
Shinkai, Y., Rathbun, G., Lam, K.P., Oltz, E.M., Stewart, V., Mendelsohn, M., et al., 1992. RAG-2-deficient mice lack mature lymphocytes owing to inability to initiate V(D)J rearrangement. Cell 68, 855–867.
Simon, K., Hennen, S., Merten, N., Blättermann, S., Gillard, M., Kostenis, E., et al., 2015. The orphan G protein-coupled receptor GPR17 negatively regulates oligodendrocyte differentiation via Gαi/o and its downstream effector molecules. J. Biol. Chem. 291, 705–718. https://doi.org/10.1074/jbc.M115.683953.
Smith, D.H., Chen, X.H., Nonaka, M., Trojanowski, J.Q., Lee, V.M., Saatman, K.E., et al., 1999. Accumulation of amyloid beta and tau and the formation of neurofilament inclusions following diffuse brain injury in the pig. J. Neuropathol. Exp. Neurol. 58, 982–992. https://doi.org/10.1097/00005072-199909000-00008.
Smith, B.M., Giddens, M.M., Neil, J., Owino, S., Nguyen, T.T., Duong, D., et al., 2017. Mice lacking Gpr37 exhibit decreased expression of the myelin-associated glycoprotein MAG and increased susceptibility to demyelination. Neuroscience 358, 49–57. https://doi.org/10.1016/j.neuroscience.2017.06.006.
Stein, T.D., Alvarez, V.E., McKee, A.C., 2014. Chronic traumatic encephalopathy: a spectrum of neuropathological changes following repetitive brain trauma in athletes and military personnel. Alzheimers Res. Ther. 6, 4. https://doi.org/10.1186/alzrt234.
Tagge, C.A., Fisher, A.M., Minaeva, O.V., Gaudreau-Balderrama, A., Moncaster, J.A., Zhang, X., et al., 2018. Concussion, microvascular injury, and early tauopathy in young athletes after impact head injury and an impact concussion mouse model. Brain 141, 422–458. https://doi.org/10.1093/brain/awx350.
Tan, X.L., Wright, D.K., Liu, S., Hovens, C., O'Brien, T.J., Shultz, S.R., 2016. Sodium selenate, a protein phosphatase 2A activator, mitigates hyperphosphorylated tau and improves repeated mild traumatic brain injury outcomes. Neuropharmacology 108, 382–393. https://doi.org/10.1016/j.neuropharm.2016.05.001.
Turner, R.C., Lucke-Wold, B.P., Logsdon, A.F., Robson, M.J., Dashnaw, M.L., Huang, J.H., 2015a. The quest to model chronic traumatic encephalopathy: a multiple model and injury paradigm experience. Front. Neurol. 6, 222. https://doi.org/10.3389/fneur.2015.00222.
Turner, R.C., Lucke-Wold, B.P., Logsdon, A.F., Robson, M.J., Lee, J.M., Bailes, J.E., et al., 2015b. Modeling chronic traumatic encephalopathy: the way forward for future discovery. Front. Neurol. 6, 223. https://doi.org/10.3389/fneur.2015.00223.
Tzekov, R., Quezada, A., Gautier, M., Biggins, D., Frances, C., Mouzon, B., et al., 2014. Repetitive mild traumatic brain injury causes optic nerve and retinal damage in a mouse model. J. Neuropathol. Exp. Neurol. 73, 345–361. https://doi.org/10.1097/NEN.0000000000000059.
Tzekov, R., Phifer, J., Myers, A., Mouzon, B., Crawford, F., 2016. Inflammatory changes in optic nerve after closed-head repeated traumatic brain injury: preliminary study. Brain Inj. 30, 1428–1435. https://doi.org/10.1080/02699052.2016.1219062.
van Eersel, J., Stevens, C.H., Przybyla, M., Gladbach, A., Stefanoska, K., Chan, C.K., et al., 2015. Early-onset axonal pathology in a novel P301S-Tau transgenic mouse model of frontotemporal lobar degeneration. Neuropathol. Appl. Neurobiol. 41, 906–925. https://doi.org/10.1111/nan.12233.
Weckbach, S., Neher, M., Losacco, J.T., Bolden, A.L., Kulik, L., Flierl, M.A., et al., 2012. Challenging the role of adaptive immunity in neurotrauma: Rag1(−/−) mice lacking mature B and T cells do not show neuroprotection after closed head injury. J. Neurotrauma 29, 1233–1242. https://doi.org/10.1089/neu.2011.2169.
Wilson, E.H., Weninger, W., Hunter, C.A., 2010. Trafficking of immune cells in the central nervous system. J. Clin. Invest. 120, 1368–1379. https://doi.org/10.1172/JCI41911.
Winston, C.N., Noël, A., Neustadtl, A., Parsadanian, M., Barton, D.J., Chellappa, D., et al., 2016. Dendritic spine loss and chronic white matter inflammation in a mouse model of highly repetitive head trauma. Am. J. Pathol. 186, 552–567. https://doi.org/10.1016/j.ajpath.2015.11.006.
Wright, D.K., O'Brien, T.J., Shultz, S.R., Mychasiuk, R., 2017. Sex matters: repetitive mild traumatic brain injury in adolescent rats. Ann. Clin. Transl. Neurol. 4, 640–654. https://doi.org/10.1002/acn3.441.
Xu, L., 2015. Animal model of repetitive mild traumatic brain injury for human traumatic axonal injury and chronic traumatic encephalopathy. Neural Regen. Res. 10, 1731–1732.
Xu, L., Nguyen, J.V., Lehar, M., Menon, A., Rha, E., Arena, J., et al., 2016. Repetitive mild traumatic brain injury with impact acceleration in the mouse: multifocal axonopathy, neuroinflammation, and neurodegeneration in the visual system. Exp. Neurol. 3, 436–449. https://doi.org/10.1016/j.expneurol.2014.11.004.
Yang, H.J., Vainshtein, A., Maik-Rachline, G., Peles, E., 2016. G protein-coupled receptor 37 is a negative regulator of oligodendrocyte differentiation and myelination. Nat. Commun. 7, 10884. https://doi.org/10.1038/ncomms10884.
Yin, Z., Valkenburg, F., Hornix, B.E., Mantingh-Otter, I., Zhou, X., Mari, M., et al., 2017. Progressive motor deficit is mediated by the denervation of neuromuscular junctions and axonal degeneration in transgenic mice expressing mutant (P301S) Tau protein. J. Alzheimers Dis. 60, S41–S57. https://doi.org/10.3233/JAD-161206.
Yoshiyama, Y., Uryu, K., Higuchi, M., Longhi, L., Hoover, R., Fujimoto, S., et al., 2005. Enhanced neurofibrillary tangle formation, cerebral atrophy, and cognitive deficits induced by repetitive mild brain injury in a transgenic tauopathy mouse model. J. Neurotrauma 22, 1134–1141. https://doi.org/10.1089/neu.2005.22.1134.
Yu, G., Wang, L., Han, Y., He, Q., 2012. clusterProfiler: an R package for comparing biological themes among gene clusters. OMICS 16, 284–287. https://doi.org/10.1089/omi.2011.0118.
Zeisel, A., Muñoz-Manchado, A.B., Codeluppi, S., Lönnerberg, P., La Manno, G., Juréus, A., 2015. Brain structure. Cell types in the mouse cortex and hippocampus revealed by single-cell RNA-seq. Science 347, 1138–1142. https://doi.org/10.1126/science.aaa1934.
Zhang, B., Gaiteri, C., Bodea, L.G., Wang, Z., McElwee, J., Podtelezhnikov, A.A., et al., 2013. Integrated systems approach identifies genetic nodes and networks in late-onset Alzheimer's disease. Cell 153, 707–720. https://doi.org/10.1016/j.cell.2013.03.030.
Zhang, Y., Chen, K., Sloan, S.A., Bennett, M.L., Scholze, A.R., O'Keeffe, S., et al., 2014. An RNA-sequencing transcriptome and splicing database of glia, neurons, and vascular cells of the cerebral cortex. J. Neurosci. 34, 11939–11947. https://doi.org/10.1523/JNEUROSCI.1860-14.2014.
Zisman, E., Waisman, A., Ben-Yair, E., Tartakovsky, B., 1993. Production of colony-stimulating factor 1 by T cells: possible involvement in their interaction with antigen-presenting cells. Cytokine 5, 309–318.
Zrzavy, T., Hametner, S., Wimmer, I., Butovsky, O., Weiner, H.L., Lassmann, H., 2017. Loss of 'homeostatic' microglia and patterns of their activation in active multiple sclerosis. Brain 149, 1899–1913. https://doi.org/10.1093/brain/awx113.